2009-01-01

An Investigation On The Mixing Hydrodynamics Of A Gas-Solid Fluidized Bed

Mario Alberto Ruvalcaba
University of Texas at El Paso, mruvalcaba@miners.utep.edu

AN INVESTIGATION ON THE MIXING HYDRODYNAMICS OF A GAS-SOLID FLUIDIZED BED

MARIO A. RUVALCABA

Department of Mechanical Engineering

APPROVED:

Ahsan Choudhuri, Ph.D., Chair

Felicia Manciu, Ph.D.

Vinod Kumar, Ph.D.

Patricia D. Witherspoon, Ph.D.
Dean of the Graduate School

DEDICATION

To my family and friends

AN INVESTIGATION ON THE MIXING HYDRODYNAMICS OF A GAS-SOLID FLUIDIZED BED

by

MARIO A. RUVALCABA, B.S.M.E.

THESIS

Presented to the Faculty of the Graduate School of

The University of Texas at El Paso

in Partial Fulfillment

of the Requirements

for the Degree of

MASTER OF SCIENCE

Department of Mechanical Engineering

THE UNIVERSITY OF TEXAS AT EL PASO

December 2009

ACKNOWLEDGEMENTS

Perhaps the most direct support to my work has come from my advisor Dr. Ahsan Choudhuri (Mechanical Engineering Department, University of Texas at El Paso). I thoroughly appreciated his patient guidance throughout this project. He helped me work in the area of my research interest in computational fluid dynamics and energy systems. His work ethic provides a great example for all the students in our group. He was also been very understanding as I went through some of the hardest times in my life and for that I am very thankful.

I would like to thank my thesis committee members, Dr. Vinod Kumar and Dr. Felicia Manciu for being on the committee and for their cooperation and suggestions.

Thanks to the financial support from the Department of Energy (DOE) and the use of the MFIX (Multiphase Flow with Interphase eXchanges) code.

Thanks to all my wonderful friends at UTEP for being there for me at all times. Also, my sincere thanks to all my teachers who have been part of my academic career.

Finally, my acknowledgments would be incomplete if I did not include my family. With the no exception any of them even know exactly what it is I do, but I could never have done it without them. My parents have encouraged me since the first grade and always given me a reason to do my best. My mother is one of the most selfless, loving people I have ever known and she has an inner strength that I can only begin to understand. All of my accomplishments are enabled by the support of my family.

ABSTRACT

In previous decades, the experimental and numerical studies of multiphase flows have remarkably increased especially gas-solid flows. Research of this type has abundant applications in energy, chemical processes, among others. Moreover, common applications include fluid catalytic cracking for petroleum refineries, fluidized bed reactors (type of chemical reactors), interface modification, such as applying a coating onto solid items, and an important technology breakthrough in coal gasification. The work presented on this thesis concentrates on the investigation of gas-solid flows utilizing Computational Fluid Dynamics (CFD) methods. The gas-solid flows studies performed on this investigation assumed the solid phase as a continuum with averaged properties and treated the gas-solid flow as constituting of interpenetrating continua.

The fluid flow computation has been achieved using two different solvers. One of them is FLUENT**,** a general-purpose CFD code based on the finite volume method on a collocated grid. FLUENT technology offers a wide array of physical models that can be applied to a wide array of industries. The other solver is MFIX (Multiphase Flow with Interphase eXchanges), a solver developed at the Department of Energy's National Energy Technology Laboratory (NETL) for multiphase flows; MFIX is a general-purpose hydrodynamic model that describes chemical reactions and heat transfer in dense or dilute fluid-solids flows, which are flows that typically occur in energy conversion and chemical processing reactors. MFIX calculations give detailed information on pressure, temperature, composition, and velocity distributions.

TABLE OF CONTENTS

LIST OF TABLES

LIST OF FIGURES

CHAPTER 1: INTRODUCTION

1.1 An Overview on Gas-Solid Flows

Multiphase flows can be classified into four categories: gas-liquid, liquid-solid, gas-solid and three phase flows. In this work gas-solid flow type is investigated. A typical example of a gas-solid flow application is a fluidized bed. Conceptually, this device consists of a vertical vessel containing a bed of particles that may range in size from microns to centimeters. A fluid (frequently a gas) is pumped through the porous bottom of the vessel, and through the bed [1]. As the gas velocity is increased, initially increasing pressures drop is observed across the bed. Nevertheless, when the pressure drop reaches a value close to the weight of the bed per unit area, the particles become suspended in the fluid stream and the bed is said to be fluidized. Numerous flow regimes are normally used to explain the characteristics of the flow through a particle bed, which include:

- Slugging bed: Bubbles of gas occupy entire fragments of the bed containment vessel and layers are created, splitting the bed into sections.
- Boiling bed: A bed in which the gas bubbles are about the same size as the solid particles.
- Channeling bed: A bed in which gas channels are formed where most of the gas flows through.
- Spouting bed: A bed in which a single gas opening is formed in which some particles flow and fall to the outside. [2]

A typical fluidized bed schematic is shown in Figure 1.1. In this system, the solid is in the form of particles that are free to move about in the reactor. Fluidized beds provide more efficient contacting between the solid and the fluid and are integral in enabling catalytic cracking to be a practical, industrial-scale process.

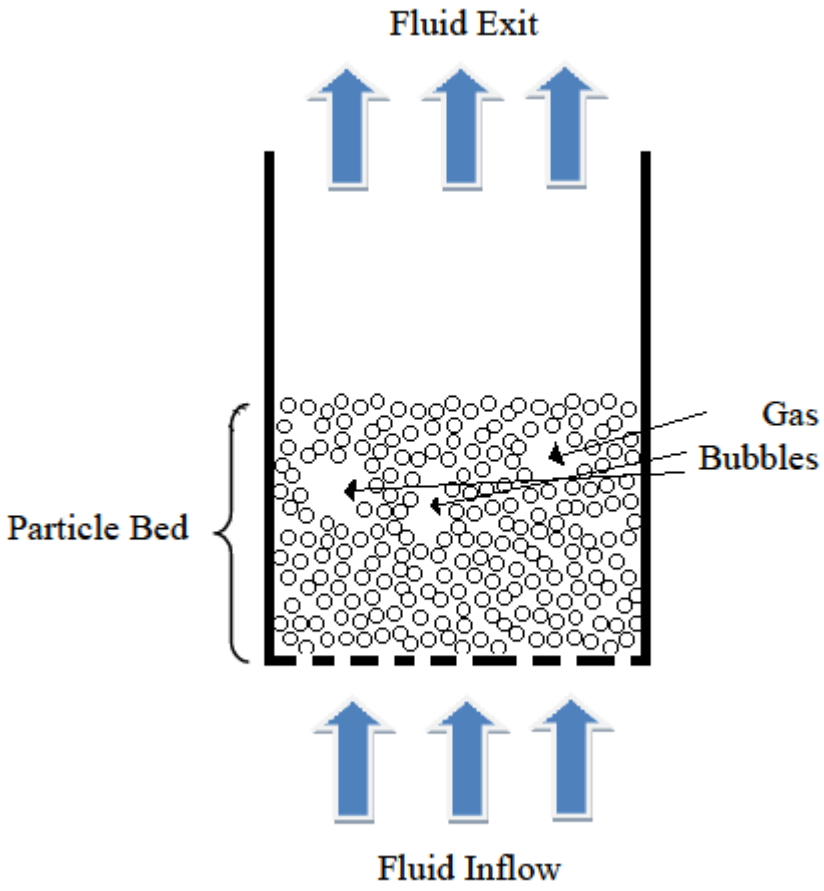

Figure 1.1: Fluidized Bed Schematic

1.2 Fluidization Particles

In 1973, Professor D. Geldart classified powders that have similar properties into four groups and designated them by the letters A, B, C, and D. This collection is called "Geldart Groups. The groups are defined by their locations on a diagram of solid-fluid density difference ($\rho_s - \rho_f$) and particle size (d_p). Moreover, fluidized bed design methodologies can be customized based upon the particle's Geldart grouping. A mapping of these groups is shown in Figure 1.2 for air fluidized beds [4].

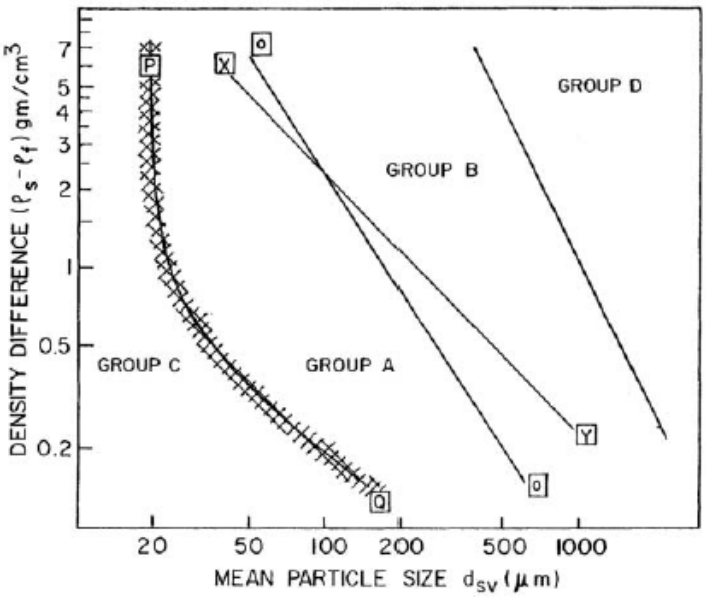

Figure 1.2: Geldart Classification of Powders [5]

Group A: "Prior to the initiation of a bubbling bed phase, beds from these particles will expand by a factor of 2 to 3 at incipient fluidization, due to a decreased bulk density. Most powder-catalyzed beds utilize this group".

Group B: "Bubbling typically forms directly at incipient fluidization".

Group C: "This group contains extremely fine and subsequently the most cohesive particles. These particles fluidize under very difficult to achieve conditions, and may require the application of an external force, such as mechanical agitation".

Group D: "Fluidization of this group requires very high fluid energies and is typically associated with high levels of abrasion. Roasting coffee beans, gasifying coals, and some roasting metal ores are such solids, and they are usually processed in shallow beds or in the spouting mode" [2].

Detailed characteristics of powders that belong to the four groups are presented in Table 1.

Table 1: Geldart's Classification of Particles [6]

	Group	
	A	**B**
Example	Cracking catalyst	Sand
Particle size (d_p), μm	30–100	$40 < d_p < 500$
Density (ρ_s), kg/m^3	<1400	1400 ð ρ_s ð 4000
Expansion	Large even before bubbling	Small
Bed collapse rate	Slow (e.g., 0.3–0.6 cm/s)	Very fast
Mixing	Rapid even with a few bubbles	Little in the absence of bubbles
Bubbles	Appear even before U_{mf} (i.e., $U_{mb}/U_{mf} > 1$)	Appear after U_{mf} (U_{mb}/U_{mf} Ý 1)
	Split and recoalesce frequently	Coalescence is predominant
	Rise velocity > interstitial gas velocity	Rise velocity > interstitial gas velocity
	For freely bubbling bed, rise velocity (30–40 cm/s) of small bubble (<4 cm) not dependent on bubble size	Size increases linearly with bed height and excess gas velocity
	Maximum bubble size exists	No evidence
	Cloud-to-bubble-volume ratio is negligible	Cloud-to-bubble-volume ratio not negligible
Slugs	Slugs produced at high superficial velocity and break	Slugs at high velocity of gas, rise along wall and no evidence of breakdown
	Slug size decreases with d_p	

	Group	
	C	**D**
Example	Finer	Coarse
Particle size (d_p), μm	<60 μm, if $(\rho_s - \rho_g) < 500$ kg/m^3, <20 μm, if $(\rho_s - \rho_g) > 1000$ kg/m^3	>500
Density (ρ_s), kg/m^3	<1400	>1400
Expansion	Powder cohesive in nature; difficult to fluidize	Solid particles are spoutable; hence expansion is similar to spouted bed
Bed collapse rate	Very poor as deaeration is not fast	Fastest of all groups because of dense or large size of particles
Mixing	Particle mixing as well as heat transfer between a surface and bed are poorer than Group A and B	Solid mixing is relatively poor; high particle momentum and little particle contact minimize agglomeration; gas velocity in dense phase is high, and hence backmixing of dense-phase gas is less
Bubbling/ fluidization	As the interparticle forces are greater than the force exerted by fluid, the powder lifts as slug in small-diameter column or channel; hence bubbling is absent or not reported	Bubbles form at 5 cm above the distributor
	Agglomeration due to excessive electrostatic force	Bubbles of similar size to those of Group B are possible at same bed height and excess gas flow rate; largest bubbles rise slower than intertitial gas, and hence gas enters the bubble base and comes out at the top
	Fluidization is generally possible by using agitator or vibrator to break the channels	
	Electrostatic charges removed by using conductive solids or solids with graphite coating or column wall with oxide coating	

1.3 Scope of the Thesis

The focus of this thesis is the numerical simulation of a gas-solid fluidized bed. Generally two different approaches may be taken to model the gas-solid flows:

Continuum Approach: This approach is regularly known as Eulerian approach. The gas and the solid are treated as interpenetrating continua. Here the continuity and momentum equations are written for each phase. This approach requires a constitutive equation for the solid phase to relate the solids stress tensor to the velocity field; the fluid phase is typically modeled as Newtonian. The interphase interaction terms often involve empirical relationships for drag, heat transfer and other exchanges [7].

Combined Continuum: Sometimes called Molecular Dynamics-MD or Discrete Element Model. Here the fluid phase is treated as before (Eulerian approach). The solid phase is not treated as a continuum. Instead, the motion of individual particle is tracked using Newton's laws, accounting for collision dynamics between particles, also including walls forces and the solid-fluid interaction forces. This approach to analyze the solid phase is known as Lagrangian approach. Other effects such as heat and mass transfer can be taken into consideration with this Eulerian-Lagrangian approach [8].

The focus of this work is the simulation of gas-solid flows in a fluidized bed using the Continuum approach, in other words Eulerian approach to represent both gas and solid phases. Moreover, different Drag correlations will be tested in order to predict the minimum fluidization characteristics.

In conclusion, CFD simulations were successfully performed. The intent of this study is to aid in better understanding and design of fluidized beds. Furthermore, other industrial applications such as coal gasification can also be studied through this type of simulations.

CHAPTER 2: LITERATURE REVIEW

2.1 Modeling of Gas-Solid Flows

Theoretical, experimental and numerical studies are being carried out by a variety of research groups to comprehend the gas-solid flow dynamics. A good general idea of work in this area may be found in Crowe, Sommerfeld and Tsuji [21]. Hydrodynamic modeling of gas-solid flows has been accepted in one form or another for over forty years now. Pritchett et al (1978) simulated a two-dimensional fluidized bed using the two-fluid model and showed the arrangement of bubbles in fluidized bed. Bouillard (1989) used a two fluid model to investigate a fluidized bed with any solid blockages inside the bed [9]. There are a number of additional studies using this approach. Detamore et al (2001) have completed an analysis of scale-up of circulating fluidized beds using kinetic theory. Major contributions to the modeling of gas-solid flows are made by Gidaspow and co-workers (Ding et al, 1990) who combined kinetic theory for the granular phase with continuum representations for the gas phase [10].

Dasgupta et al (1994, 1998) have developed model for gas-particle flow in a vertical channel. For the solid stress tensor they used the Newtonian model. In such flows, when the particle number increases, the inertial and viscous effects are dominated by the inter-particle collisions. Glasser et al (1995, 1997, 1998) have performed theoretical studies and computed the solutions for one-dimensional and two-dimensional traveling wave solutions for the equations of motion for gas and particles in a fluidized bed. They used the Newtonian model for the solid stress tensor. They found that the solutions for fully developed two dimensional waves capture the bubble phenomenon in fluidized beds. In fluidized beds regions of high and low particle concentration are seen to form sporadically. The regions of low particle concentration are known as bubbles and those of high particle concentration are called clusters. They have also proposed a non-dimensional number whose value indicates whether bubbles

form or not. This non-dimensional value depends on the density of the particles, the terminal settling velocity of a particle, gravity and particle phase viscosity [9].

2.2 Multiphase Flow with Interphase eXchanges (MFIX) Code

The theoretical and numerical foundations of MFIX are based on a hydrodynamic theory of fluidization. Hydrodynamic models have been developed and applied to describe fluidization since the early 60's for instance Davidson and Harrison in 1963, among others. In those studies, the hydrodynamic models were used to study the stability of fluidization; no attempt was made to solve the rather fearsome set of partial differential equations constituting the model. Nonetheless, the advent of high-speed computers prompted attempts to solve these equations numerically. In the late 70's, some projects funded by the U.S. Department of Energy (DOE) were initiated to develop computer models based on the hydrodynamic equations, the CHEMFLUB code, and the FLAG code. These codes solve continuum equations to describe gas flow, but use a particle-tracking method to describe solids flow (Scharff et al. 1982). To some extent in parallel to those efforts, Professor Gidaspow and at the Illinois Institute of Technology (IIT) began to develop computer codes for describing fluidized beds [11].

In addition, Hydrodynamic modeling has the ability to reproduce data from various simple experiments (for example, the drag on an isolated sphere). Time dependent allocation of fluid and solids volume fractions, velocities, pressure, etc, can be described where measurement of such quantities in real life is impossible. These calculations, allow understanding of how parameters vary as operating conditions are changed. However, with such power also come several limitations that the user must bear in mind. First, the accuracy of the model's predictions may be limited for some reasons, such as: imperfect formulation of the governing equations, deficient knowledge of the constitutive relations, inadequate numerical treatment of the governing partial differential equations, and deficient information on initial and boundary conditions. This implies the need for much caution when performing simulations

and interpreting results. A second limitation of hydrodynamic modeling is that a user is needed to carry out simulations and to to examine results. To help the user, MFIX accounts for these difficulties in setting up simulations by using a special NAMELIST format in the input file that notifies input errors and allows comment lines. There is no limitation on the number of initial and boundary conditions. Finally, a third limitation is that hydrodynamic modeling requires significant computer resources. The availability of faster and more sophisticated computers has made hydrodynamic modeling more affordable [11].

CHAPTER 3: FLUIDIZATION

3.1 Fluidized Bed Behavior

Once the fluid flow rate is increased to produce incipient fluidization, this flow rate value is quoted as a velocity is termed “minimum fluidization velocity”, U_{mf}, defined as

$$U_{mf} = \frac{\dot{V}_{mf}}{A} \tag{3.1}$$

Where $\dot{V}_{mf}$ is the volume flow rate at incipient fluidization and A is the cross-sectional area of the bed containment [12].

Figure 3.1 shows how the pressure drop across the bed changes with respect to the gas velocity.

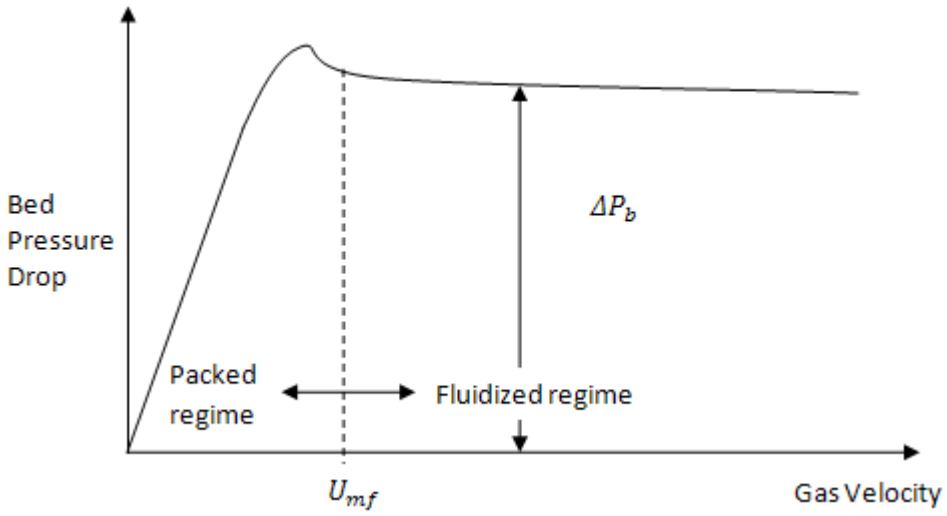

Figure 3.1: Bed Performance with Respect to the Gas Velocity

3.2 Bed Pressure Drop

Once fluidization has been achieved, the pressure drop across the bed, ΔP_b , will be sufficient to support the particle weight, thus

$$\Delta P_b = \frac{M}{\rho_p A}\left(\rho_p - \rho_f\right)g \tag{3.2}$$

Where M is the mass of the particles, ρ_p is the particle density, ρ_f is the fluid density, A is the cross-sectional area of the bed containment and g is the gravitational constant [12].

If the density of the fluid is negligible compared to the one of the particles, Equation (3.2) can be simplified to

$$\Delta P_b = \frac{Mg}{A} \tag{3.3}$$

3.3 Flow Modeling

The approach used by Ergun and Orning (1949) modeled a packed bed as a series of identical, straight, parallel channels, and then to form an equation of the form, pressure gradient:

$$\frac{dp}{dx} = av + bv\text{^}2 \tag{3.4}$$

Where v is the fluid velocity through the channels and a and b are coefficients. The first and second terms in equation (3.4) are subsequently multiplied by the dimensionless correlation factors α and β, respectively [12].

Thus

$$\frac{dp}{dx} = \alpha a v + \beta b v\text{^}2 \tag{3.5}$$

Values of α and β were determined by conducting experiments. The coefficient a was obtained from the well known Hagen-Poiseuille equation for Pressure Drop, ΔP_v , over the length, L , of a single straight tube of circular cross section of diameter d , in which the flow is entirely laminar, thus

$$\frac{\Delta P_v}{L} = \frac{32\,\mu_f\, v}{d^2} \tag{3.6}$$

where v is the mean fluid velocity thorugh the tube and μ_f is the viscosity.

The pressure drop ΔP_k due to dissipation of kinetic energy in eddies or turbulence will be

$$\frac{\Delta P_k}{L} = \tfrac{1}{2}\rho_f v^2 \frac{f}{L} \tag{3.7}$$

Where f is a dimensionless friction factor, taken in this case as being equal to L/d .

The total pressure drop ΔP_b over the length L is therefore

$$\frac{\Delta P_b}{L} = 32\,\mu_f \frac{v}{d^2} + \frac{1}{2d}\rho_f v^2 \tag{3.8}$$

If the bed is considered to be composed of N such tubes in parallel, then their length L and diameter d can be expressed in terms of the surface area and volume of solid particles in the bed and the bed voidage.

The surface area of the tube walls:

$$A_w = N\pi dL \tag{3.9}$$

And the volume of the fluid in the tubes

$$V_f = \frac{N\pi d^2 L}{4} \tag{3.10}$$

Thus

$$\frac{surface\ area\ of\ tube\ walls}{volume\ of\ fluid\ in\ tubes}, \frac{A_w}{V_f} = \frac{4}{d} \tag{3.11}$$

If the bed of particles is of depth, containment diameter D and voidage ε then the surface area of particles

$$= \sum(n_p s_p) \tag{3.12}$$

Where n_p and s_p are the number and surface area of particles of each size,p, in the bed, the volume of solid particles

$$= \sum(n_p v_p) = (1-\varepsilon)\frac{\pi}{4}D^2 L \tag{3.13}$$

Where v_p is the volume of each particle of each size and the volume of voids

$$= \varepsilon\frac{\pi}{4}D^2 L \tag{3.14}$$

Now the surface-to-void volume of the bed, S_{vv} , is to be the same as that of the cluster of tubes,

$$= 4\sum(n_p v_p)\,(\varepsilon\pi D^2 L)^{-1} = \frac{4}{d} \tag{3.15}$$

However, from eqn. (3.11)

$$\pi D^2 L = \left(4\sum(n_p v_p)\right)(1-\varepsilon)^{-1} \tag{3.16}$$

Inserting this into eqn. (3.13) gives

$$d = \left(\frac{4\varepsilon}{1-\varepsilon}\right)/(\text{surface: volume ratio Sv of the particles}) \tag{3.17}$$

$$= \left(\frac{4\varepsilon}{1-\varepsilon}\right)\frac{1}{s_v} \tag{3.18}$$

Now the fluid velocity v, through the voids, is related to a superficial fluidizing velocity U by

$$v = \frac{U}{\varepsilon} \tag{3.19}$$

Substituting for v and d in eqn. (3.8) leads

$$\frac{\Delta P_b}{L} = \frac{2\,(1-\varepsilon)^2}{\varepsilon^2}\mu_f {s_v}^2 U + \frac{1}{8}\frac{(1-\varepsilon)}{\varepsilon^3}\rho_f s_v U^2 \tag{3.20}$$

Inserting the dimensionless correlation factors α and β gives

$$\frac{\Delta P_b}{L} = 2\alpha\frac{(1-\varepsilon)^2}{\varepsilon^2}\mu_f {s_v}^2 U + \frac{\beta}{8}\frac{(1-\varepsilon)}{\varepsilon^3}\rho_f s_v U^2 \tag{3.21}$$

Ergun (1952) took the matter further; pointing out that it is customary to use a particle mean size d_m in pressure drop calculations. For spherical particles

$$d_m = \frac{6}{S_v} \tag{3.22}$$

Substitution of this into eqn. (3.21) gives

$$\frac{\Delta P_b}{L} = 72\alpha\ \frac{(1-\varepsilon)^2}{\varepsilon^2}\frac{\mu_f U}{{d_m}^2} + \frac{3\beta}{4}\frac{(1-\varepsilon)}{\varepsilon^3}\rho_f\frac{U^2}{d_m} \tag{3.23}$$

(If particles are non-spherical and are of sphericity φ and mean size d then d_m in eqn. (20) is replaced by the product $\varphi\, d$.)

Dividing each side of the eqn. (3.23) by $(1-\varepsilon)^2\mu_f U/\varepsilon^3 {d_m}^2$ gives

$$\frac{\Delta P_b \varepsilon^3 {d_m}^2}{L\mu_f U(1-\varepsilon)^2} = 72\alpha + \frac{3\beta}{4}\frac{1}{(1-\varepsilon)}\frac{\rho_f U d_m}{\mu_f} \tag{3.24}$$

Where $\rho_f U d_m/\mu_f$ is the particle Reynolds Number Re_p.

Ergun plotted a large amount of data from experiments with different types and sizes of particle and different fluids using equation (3.24). The values of 72α and 3β/4 were found to be 150 and 1.75 respectively. Therefore equation (3.24) is rearranged in the following fashion also for non-spherical particles of sphericity φ:

$$\frac{\Delta P_b}{L} = 150\ \frac{(1-\varepsilon)^2}{\varepsilon^3}\frac{\mu_f U}{(\varphi\, d_m)^2} + 1.75\ \frac{(1-\varepsilon)}{\varepsilon^3}\frac{\rho_f U^2}{\varphi\, d_m} \tag{3.25}$$

Eqn. (3.25) is commonly known as the "Ergun equation". The first term of the equation is linear in U and this is dominant when the flow in the voids is laminar. The second term is referred to turbulence [12].

3.4 Theoretical Determination of the Minimum Fluidization Velocity

By equating the Pressure drop across a packed bed, given by the Ergun equation to that of a fluidized bed, and solving for the velocity U, the obtained value will be the minimum fluidization velocity U_{mf}. The previous approach was suggested by Ergun and Orning (1949) [12].

Moreover, substituting $(1-\varepsilon)(\rho_p-\rho_f)gL$ (where g is the gravitational acceleration) for ΔP_b , ε_{mf} for ε, and U_{mf} for U in equation (3.25) lead to:

$$(1-\varepsilon)(\rho_p-\rho_f)gL = 150\,\frac{(1-\varepsilon_{mf})^2}{\varepsilon_{mf}{}^3}\frac{\mu_f U_{mf}}{(\varphi\, d_m)^2} + 1.75\,\frac{(1-\varepsilon_{mf})}{\varepsilon_{mf}{}^3}\frac{\rho_f U_{mf}{}^2}{\varphi\, d_m} \tag{3.26}$$

Multiplying each side by $\rho_f d_m{}^3/\mu_f{}^2(1-\varepsilon_{mf})$ gives

$$\frac{\rho_f(\rho_p-\rho_f)g d_m{}^3}{\mu_f{}^2} = 150\,\frac{(1-\varepsilon_{mf})}{\varphi^2\varepsilon_{mf}{}^3}\frac{\rho_f U_{mf} d_m}{\mu_f} + \frac{1.75}{\varphi\varepsilon_{mf}{}^3}\frac{\rho_f{}^2 U_{mf}{}^2 d_m{}^2}{\mu_f{}^2} \tag{3.27}$$

The left-hand side of eqn. (3.27) is the dimensionless number known as the Archimedes Number, Ar:

$$Ar = \frac{\rho_f(\rho_p-\rho_f)g d_m{}^3}{\mu_f{}^2} \tag{3.28}$$

On the right-hand side of Eqn. (3.27) appears the Reynolds Number based on the minimum fluidization velocity and particle diameter. Thus:

$$Ar = 150\,\frac{(1-\varepsilon_{mf})}{\varphi^2\varepsilon_{mf}{}^3}\,Re_{mf} + \frac{1.75}{\varphi\varepsilon_{mf}{}^3}\,Re_{mf}{}^2 \tag{3.29}$$

Furthermore, Wen and Yu were the first to use this type of correlation and to solve it for Re_{mf}. In order to arrive at a suitable solution, Wen and Yu collected the data for ε_{mf} and φ_s and the following approximations were found:

$$\frac{(1-\varepsilon_{mf})}{\varphi^2\varepsilon_{mf}{}^3} \cong 11 \text{ and } \frac{1.75}{\varphi\varepsilon_{mf}{}^3} \cong 14 \tag{3.30}$$

The Wen and Yu correlation expressed using Re_{mf} and Ar is

$$Ar = 24.5Re_{mf}{}^2 + 1650Re_{mf} \tag{3.31}$$

The solution for Re_{mf}, which has the form given in eqn. (3.29), can be written as:

$$Re_{mf} = \left((A_1 + B_1 Ar)\right)^{1/2} - A \tag{3.32}$$

The values of A_1 and B_1 depend on the experimental conditions and the range of Re_{mf}. The values of constants A_1 and B_1 in eqn. (3.32) that satisfy the various correlations reported in the literature by various researchers are presented in Table 2 [6].

Table 2: Basic Form of Correlations for Re*mf* Derived from Pressure Drop Principles [6]

Correlation: $Re_{mf} = (A_1^2 + B_1 Ar)^{1/2} - A_1$, $\alpha = (1-\epsilon)/\phi_s^2 \epsilon^3$, $\beta = 1/(\phi_s \epsilon^3)$, $m = \alpha/\beta$				
	Constants			
Ref.	A_1	B_1	m	Remarks
Ergun[42]	42.85/α	0.57/β	$(1-\epsilon)/\phi_s$	Modified for fluidized bed
Wen and Yu[33]	33.7	0.0408	0.7857	Water-fluidized, spherical particle
Bourgeois and Grenier[44]	25.46	0.0382	0.594	Spherical particle
Ghosal and Mukherjee[45]	29.2	0.029	0.6814	For spherical and angular ($1 < Re_{mf} < 1000$)
Saxena and Vogel[46]	25.28	0.0571	0.5899	Air fluidized, $6 < Re_{mf} < 102$
Babu et al.[47]	25.25	0.0651	0.5892	High pressure (7000 kPa) for coal gasification
Richardson and Jeromino[48]	25.7	0.0365	0.5997	
Thonglimp et al.[49]	19.9	0.03196	0.4644	Binary system
Chitester et al.[50]	28.7	0.0494	0.6697	High-pressure fluidization (6485 kPa)
Thonglimp et al.[30]	31.6	0.0925	0.7374	Air fluidized
Masaaki et al.[51]	33.95	0.0465	—	Elevated temperature (280–800 K) and pressure (0.1–4.9 MPa)
Agarwal and O'Neil[52]	42.81	0.061	0.999	—
Satyanarayana and Rao[53]	30.10	0.0417	0.7024	Elevated temperature (295–490 K)
Grace[54]	27.2	0.0408	0.635	Correlation from literature
Panigrahi and Murty[55]	32.2	0.0382	0.751	Trial-and-error method adopted to develop general correlation for spherical multiparticle drag coefficient

CHAPTER 4: SIMULATION PHASE MODELS

4.1 Gas-Phase Governing Equations

4.1.1 Volume Fraction Equation

By means of the averaging approach to model equations, new filed variables are introduced. These are the phasic volume fractions; they represent the fraction of averaging the volume taking place by various phases. By concept, the volume fractions of all the phases must add to one:

$$\varepsilon_g + \varepsilon_s = 1 \tag{4.1}$$

where ε_g is the volume for the fluid phase, also known as the void fraction, and ε_s , the volume fraction for the solid phase [11].

4.1.2 Continuity Equation

The fluid phase is modeled by solving an average mass and momentum balance. The continuity equation is given by:

$$\frac{\partial}{\partial t}\left(\varepsilon_g\, \rho_g\right) + \nabla \cdot \left(\varepsilon_g\, \rho_g \overrightarrow{v_g}\right) = 0 \tag{4.2}$$

where ε_g is the void fraction, ρ_g is the gas density and $\overrightarrow{v_g}$ is the gas velocity. The first term in equation (1) represents the increase of mass per unit volume and the second term represents the flux of convective mass per unit volume [13].

4.1.3 Momentum Equation

The balance of momentum is given by

$$\frac{\partial}{\partial t}\left(\varepsilon_g\, \rho_g \overrightarrow{v_g}\right) + \nabla \cdot \left(\varepsilon_g\, \rho_g \overrightarrow{v_g}\, \overrightarrow{v_g}\right) = \nabla \cdot \overline{\overline{S_g}} + \varepsilon_g\, \rho_g \vec{g} - \overrightarrow{I_{gs}} \tag{4.3}$$

where the first term on the left-hand side refers to the increase of momentum per unit volume and the second term refers to the rate of momentum gain by convection per unit volume. On the right-hand side, the first term describes the rate of momentum transfer by normal and shear stress components per unit

volume; $\overline{\overline{S_g}}$ is the gas-phase stress tensor, the second term explains the net gravitational force on the fluid per unit volume; $\vec{g}$ is the acceleration due to gravity, and the last term represents the interaction force between the fluid and solid phases per unit volume; $\overrightarrow{I_{gs}}$ is the rate of momentum transfer between the gas and solid phase per unit volume [11].

The gas-solid momentum transfer is described by:

$$\overrightarrow{I_{gs}} = -\varepsilon_s \nabla P_g - F_{gs}\left(\overrightarrow{v_s} - \overrightarrow{v_g}\right) \tag{4.4}$$

where P_g is the gas-phase pressure and $\overrightarrow{v_s}$ is the average solids velocity. The drag coefficient F_{gs} is determined by two types of experimental data. One type is available as correlations for the terminal velocity. In fluid dynamics an object is moving at its *terminal velocity* if its speed is constant due to the restraining force exerted by the air, water or other fluid through which it is moving. A free-falling object achieves its terminal velocity when the downward force of gravity (weight) equals the upward force of drag. This causes the net force on the object to be zero, resulting in an acceleration of zero.

4.2 Drag Correlations

4.2.1 Syamlal-Obrien Correlation

Syamlal and O'brien derived the following equation for converting terminal velocity correlations to drag correlations [14]:

$$F_{gs} = \frac{3\varepsilon_s \varepsilon_g \rho_g}{4{v_t}^2 d_p} C_{D-sphere}\left|\overrightarrow{v_s} - \overrightarrow{v_g}\right| \tag{4.5}$$

where d_p is the particle diameter and v_t is the terminal velocity . The single-sphere drag coefficient $C_{D-sphere}$ is defined by the formula given by Dalla Valle [15]:

$$C_{D-sphere} = \left(0.63 + 4.8\sqrt{\frac{v_t}{Re}}\right)^2 \tag{4.6}$$

The terminal velocity v_t is described by the following correlation modeled by Garside and Al-Dibouni [16]:

$$v_t = 0.5\left(A - 0.06Re + \sqrt{(0.06Re)^2 + 0.12Re(2B - A) + A^2}\right) \tag{4.7}$$

where

$$A = {\varepsilon_g}^{4.14} \tag{4.8}$$

$$B = \begin{cases} 0.8{\varepsilon_g}^{1.28} & \varepsilon_g \leq 0.85 \\ {\varepsilon_g}^{2.65} & \varepsilon_g > 0.85 \end{cases} \tag{4.9}$$

and the Reynolds number, Re is defined as

$$Re = \frac{d_p|\overrightarrow{v_s} - \overrightarrow{v_g}|\rho_g}{\mu_g} \tag{4.10}$$

where μ_g is the gas viscosity [17].

4.2.2 Gidaspow Correlation

The other type of data available for drag formulation, is valid for high value of solids volume fraction, is packed-bed pressure data expressed in the form of a correlation, such as the Ergun equation. Such a correlation must be complemented with a drag correlation for low values of the solids volume fraction. Such correlation is the Gidaspow drag correlation [18]:

$$F_{gs} = \begin{cases} \frac{3}{4} C_{D-sphere} \frac{\rho_g \varepsilon_g \varepsilon_s |\overrightarrow{v_s} - \overrightarrow{v_g}|}{d_p} {\varepsilon_g}^{-2.65} & \varepsilon_g \geq 0.8 \\ \frac{150\varepsilon_s(1-\varepsilon_g)\mu_g}{\varepsilon_g {d_p}^2} + \frac{1.75\rho_g \varepsilon_s |\overrightarrow{v_s} - \overrightarrow{v_g}|}{d_p} & \varepsilon_g < 0.8 \end{cases} \tag{4.11}$$

The single-sphere drag coefficient $C_{D-sphere}$ is defined by the formula

$$C_{D-sphere} = \begin{cases} 24/Re(1 + 0.15Re^{0.687}) & Re \leq 1000 \\ 0.44 & Re > 1000 \end{cases} \tag{4.12}$$

and the Reynolds number, Re is defined as

$$Re = \frac{\varepsilon_g \rho_g |\overrightarrow{v_s} - \overrightarrow{v_g}| d_p}{\mu_g} \tag{4.13}$$

4.3 Solid-Phase Governing Equations

4.3.1 Continuity Equation

The solid phase is modeled by solving an average mass and momentum balance. The continuity equation is given by:

$$\frac{\partial}{\partial t}(\varepsilon_{sm}\,\rho_{sm}) + \nabla\cdot(\varepsilon_{sm}\,\rho_{sm}\overrightarrow{v_{sm}}) = 0 \tag{4.14}$$

where ε_{sm} is the m[th] solids volume fraction, ρ_s is the m[th] solids density and $\overrightarrow{v_s}$ is the m[th] solids velocity. The first term in equation (1) represents the increase of mass per unit volume and the second term represents the flux of convective mass per unit volume [16].

4.3.2 Momentum Equation

The balance of momentum is given by

$$\frac{\partial}{\partial t}(\varepsilon_{sm}\,\rho_{sm}\overrightarrow{v_{sm}}) + \nabla\cdot(\varepsilon_{sm}\,\rho_{sm}\overrightarrow{v_{sm}}\,\overrightarrow{v_{sm}}) = \nabla\cdot\overline{\overline{S_{sm}}} + \varepsilon_{sm}\,\rho_{sm}\vec{g} + \overrightarrow{I_{gs}} - \overrightarrow{I_{ml}} \tag{4.15}$$

where the first term on the left-hand side refers to the increase of momentum per unit volume and the second term refers to the rate of momentum gain by convection per unit volume. On the right-hand side, the first term describes the rate of momentum transfer by normal and shear stress components per unit volume; $\overline{\overline{S_{sm}}}$ is the m[th] solids stress tensor, the second term explains the net gravitational force on the solids per unit volume; $\vec{g}$ is the acceleration due to gravity, the next term represents the interaction force between the fluid and m[th] solid phase per unit volume; $\overrightarrow{I_{gs}}$ is the rate of momentum transfer between the gas and solid phase per unit volume, and the last term $\overrightarrow{I_{ml}}$ is the rate of momentum transfer between the different solid phases per unit volume.

The gas-solid momentum transfer is described by:

$$\overrightarrow{I_{ml}} = F_{ml}(\overrightarrow{v_{sl}} - \overrightarrow{v_{sm}}) \tag{4.16}$$

where $\overrightarrow{v_{sl}}$ is the average solids velocity for the l[th] solid phase, $\overrightarrow{v_{sm}}$ is the average solids velocity for the m[th] solid phase The drag coefficient F_{sl} is represented by a relation derived by Syamlal:

$$F_{ml} = \frac{3(1+e_{lm})(\pi/2+C_{f-lm}\pi^2/8)\varepsilon_{sl}\rho_{sl}\varepsilon_{sm}\rho_{sm}(d_{pl}+d_{pm})^2 g_{o-lm}|\overrightarrow{v_{sl}}-\overrightarrow{v_{sm}}|}{2\pi(\rho_{sl}{d_{pl}}^3+\rho_{sm}{d_{pm}}^3)} \quad (4.17)$$

where e_{lm} and C_{f-lm} are the coefficient of restitution and the coefficient of friction, between the l[th] and m[th] solid phase particles. The radial distribution function g_{o-lm} is a correction factor that modifies the probability of collisions between grains when the solid granular phase becomes dense. The following equation was derived by Lebowitz for a mixture of hard spheres [19]:

$$g_{o-lm} = \frac{1}{\varepsilon_g} + \frac{3d_{pl}d_{pm}}{{\varepsilon_g}^2(d_{pl}+d_{pm})}\sum_{n=l}^{M}\frac{\varepsilon_{sn}}{d_{pn}} \quad (4.18)$$

4.4 Modeling Turbulence: The *k*-ε model

The *k*-ε model belongs to the class of *two-equation models*, in which model transport equations are solved for two turbulence quantities-i.e. *k* and ε in the *k*-ε model. From these two quantities can be formed a lengthscale ($L = k^{3/2}/\varepsilon$), a timescale ($\tau = k/\varepsilon$), a quantity of dimension $\nu_T(k^2/\varepsilon)$. As a consequence, two-equation models can be complete-flow-dependent specifications such as a mixing length ($l_m(x)$) are not required [20].

The two transport equations are the following:

$$\frac{\bar{D}k}{\bar{D}t} = \nabla\cdot\left(\frac{\nu_T}{\sigma_k}\nabla k\right) + P - \varepsilon \quad (4.19)$$

$$\frac{\bar{D}\varepsilon}{\bar{D}t} = \nabla\cdot\left(\frac{\nu_T}{\sigma_\varepsilon}\nabla\varepsilon\right) + C_{\varepsilon 1}\frac{P\varepsilon}{k} - C_{\varepsilon 2}\frac{\varepsilon^2}{k} \quad (4.20)$$

Where k is the turbulent kinetic energy, ε turbulent dissipation rate, P is the turbulence production, ν_T is the turbulent viscosity, and σ_k the turbulent Prandtl number.

The standard values of all model constants are

$$C_{\mu}=0.09, \quad C_{\varepsilon 1}=1.44, \quad C_{\varepsilon 2}=1.92, \quad \sigma_{k}=1.0, \quad \sigma_{\varepsilon}=1.3 \tag{4.21}$$

CHAPTER 5: FLUIDIZED BED SIMULATION

5.1 Problem Setup

The bed consists of 1mm spherical Borosilicate glass beads. Borosilicate glass is widely used for laboratory glassware, either mass produced or as custom made. Borosilicate glass has excellent thermal properties with its low coefficient of expansion and high softening point, it also offers a high level of resistance to attack from water, acids, salt solutions, organic solvents and halogens. Resistance to alkaline solutions is moderate and strong alkaline solutions cause rapid corrosion of the glass, as does Hydrofluoric acid and hot concentrated Phosphoric acid. Table 3 shows the physical properties of Borosilicate glass.

Table 3: Borosilicate Glass Physical Properties

Physical Properties	
SiO2 = 80.6%	Coefficient of expansion (20°C–300°C) 3.3 x 10-6 K-1
B2O3 = 13.0%	Density 2.23g/cm3
Na2O = 4.0%	Refractive index (Sodium D line) 1.474
Al2O3 = 2.3%	Dielectric constant (1MHz, 20°C) 4.6
Optical Information	Specific heat (20°C) 750J/kg°C
Refractive index (Sodium D line) = 1.474	Thermal conductivity (20°C) 1.14W/m°C
Visible light transmission, 2mm thick glass = 92%	Poisson's Ratio (25°C – 400°C) 0.2
Visible light transmission, 5mm thick glass = 91%	Young's Modulus (25°C) 6400 kg/mm2

Moreover, the particle containment is a cylindrical vessel of 3.2cm (1.25 inches) diameter and 183cm (72 inches) of height. However, for the computational analysis only 30 cm of the vessel height were considered. In addition, the static bed height analyzed was 5 cm. As shown in Figure 5.1.

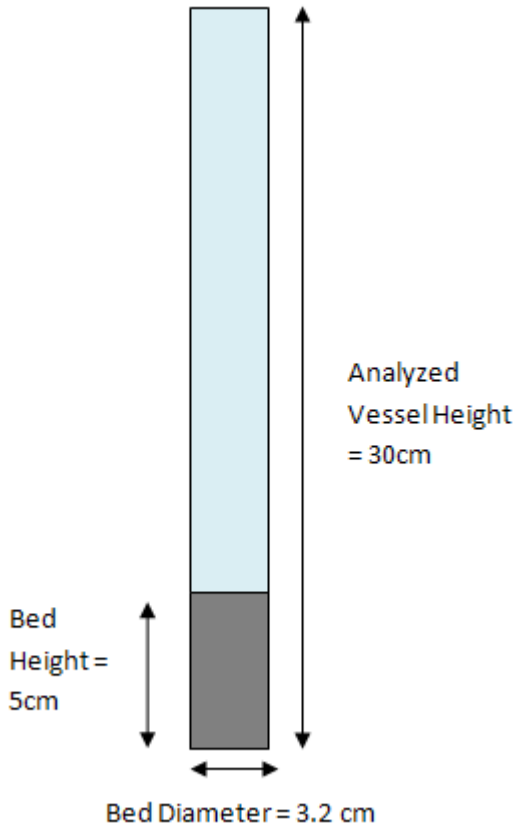

Figure 5.1: Particle Bed Setup

5.2 Computational Grid

The fluid simulation domain consists of a three-dimensional cylindrical system with the origin of the *x-, y-* and *z-* axis centered at the bottom of the cylinder, as shown in Figure 5.1.

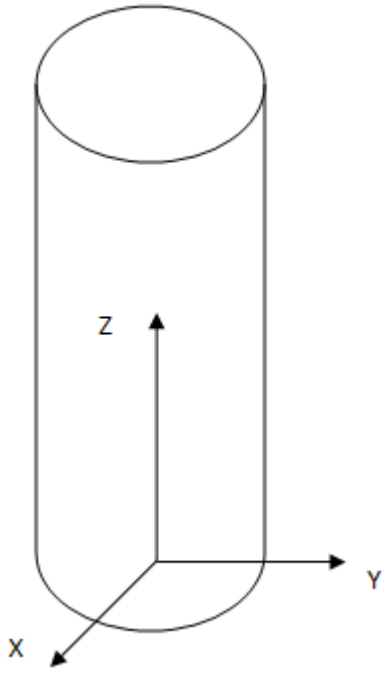

Figure 5.2: Bed Coordinate System

As previously mentioned the bed dimensions for the analysis are 3.2 cm in diameter by 30 cm of height. For this design, three computational grids were generated; two for the Fluent CFD and one for MFIX Code.

For the Fluent Code, the first computational grid contained 13400 cells. A second grid was generated, but now containing a finer mesh. A total of 154200 cells were generated. Figures 5.2 and 5.3 show the Fluent computational grids.

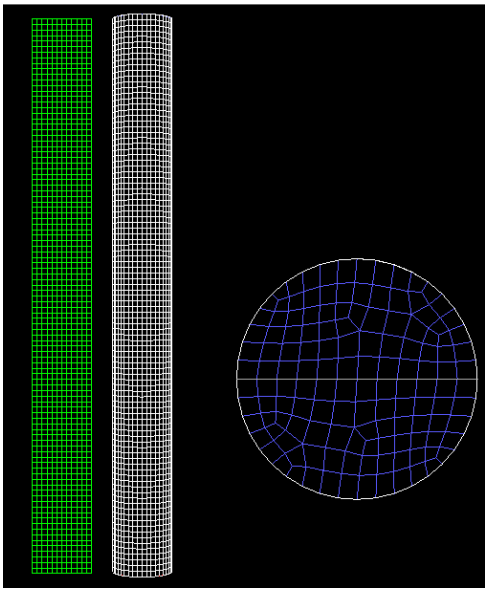

Figure 5.3: Coarse-Grid

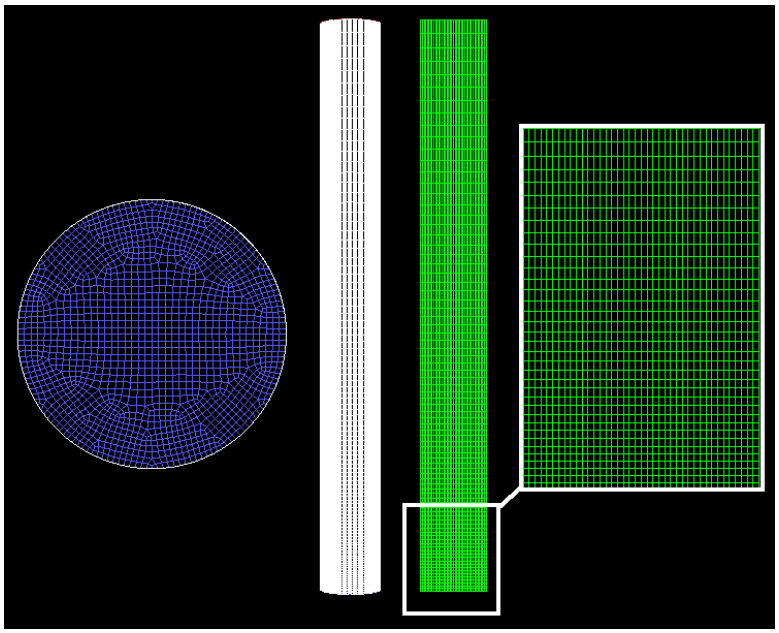

Figure 5.4: Fine-Grid

For the MFIX Code, the computational grid consists of 6 cells in the radial direction, 50 cells in the axial direction and 8 cells azimuthally. Figure 5.4 shows the MFIX computational grid.

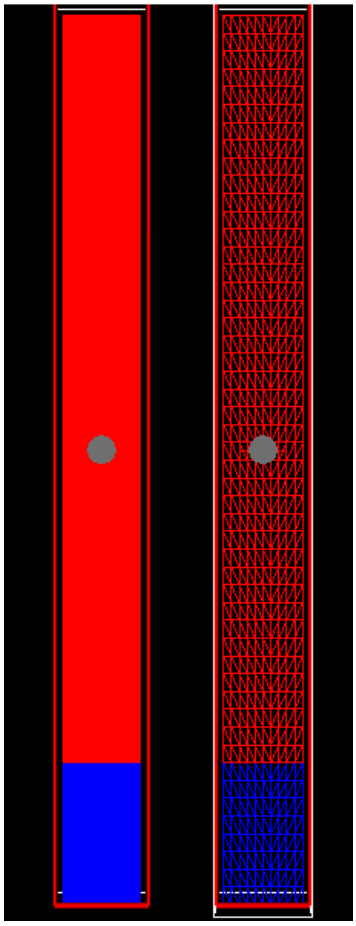

Figure 5.5: MFIX Grid

5.3 Boundary and Initial Conditions

For the initial conditions in MFIX, the bed is divided into a “bed” section and a “freeboard” section with the former taking up the bottom half of the bed and the latter comprising the top half. In the bed section, the gas void fraction is initially set to 0.45, which is a typical value at minimum fluidization. The gas velocity is initially set to 10 cm/s in the *y*-direction. In the freeboard section the void fraction is initially set to unity and the *y*-component of the gas velocity is initially set to 45.8. In order to produce fluidization curves, most simulations are run with inlet conditions that vary with time and the initial conditions have essentially no effect on these results. The boundary conditions for the gas phase consist of no-slip, impermeable walls on the vertical sides of the bed. For the outflow boundary

condition at the top of the bed, zero gauge pressure is specified across the entire width. At the boundary condition of the velocity inlet, the void fraction is set to unity and the gas velocity is set to achieve the desired superficial velocity in the bed.

For the initial conditions in Fluent, the bed is divided into a "bed" region and a "freeboard" region with the former taking up the bottom half of the bed and the latter comprising the top half. In the bed region, the solids void fraction is initially set to 0.55, since Fluent handles solids volume fraction instead of gas volume fraction as MFIX. The gas velocity is initially set to 10 cm/s in the z-direction. In order to produce fluidization curves, most simulations are run with inlet conditions that vary with time and the initial conditions have essentially no effect on these results. The boundary conditions for the gas phase consist of no-slip, impermeable walls on the vertical sides of the bed. For the outflow boundary condition at the top of the bed, a Pressure Outlet set at atmospheric pressure (101.325 KPa) is specified across the entire width. At the Bed Inlet, a velocity inlet boundary condition is specified.

5.4 Simulation Procedure

The procedure in which the analyses were conducted is shown in Figure 5.6:

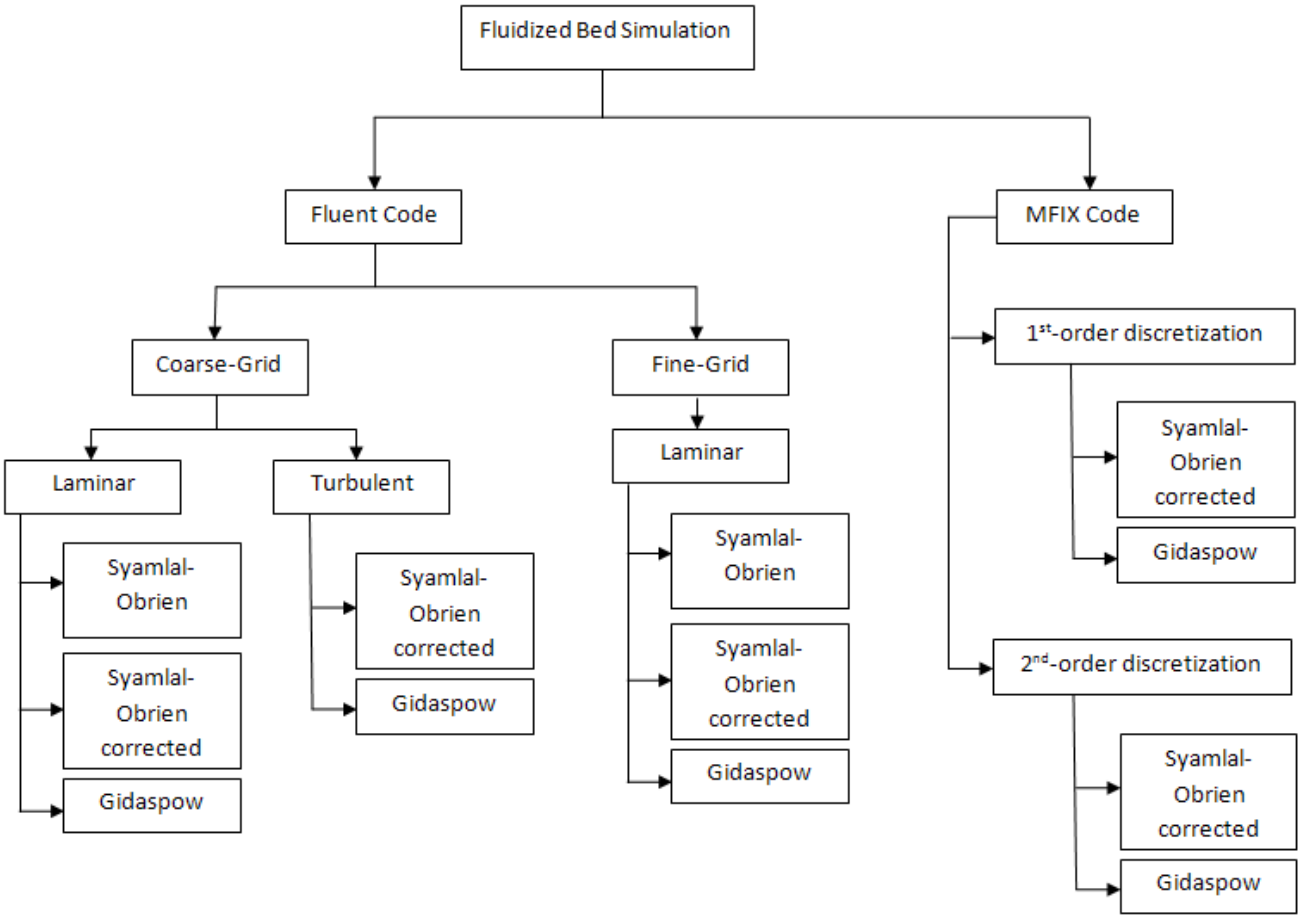

Appendix:

- Syamlal-Obrien Corrected

Figure 5.6: Simulation Procedure Schematic

5.5 Results

A series of fluidization curves were obtained for each different interaction of flow regime (laminar or turbulent), computational grid (coarse or fine), and Drag correlation (Syamlal-Obrien, Syamlal-Obrien corrected and Gidaspow). Furthermore, at each simulation run a fluidization curve was obtained, all this by increasing the gas velocity in different steps. In addition, all the analyses were run using the 'cgs' unit system. The run time for all simulations was for 1 second at a constant time-step.

5.5.1 Fluent Code Results

The following values were obtained by Fluent in order to design the fluidization curves. Each interaction of flow factors is shown in the next charts. The run time was for 1 second with a time-step of 0.001 s.

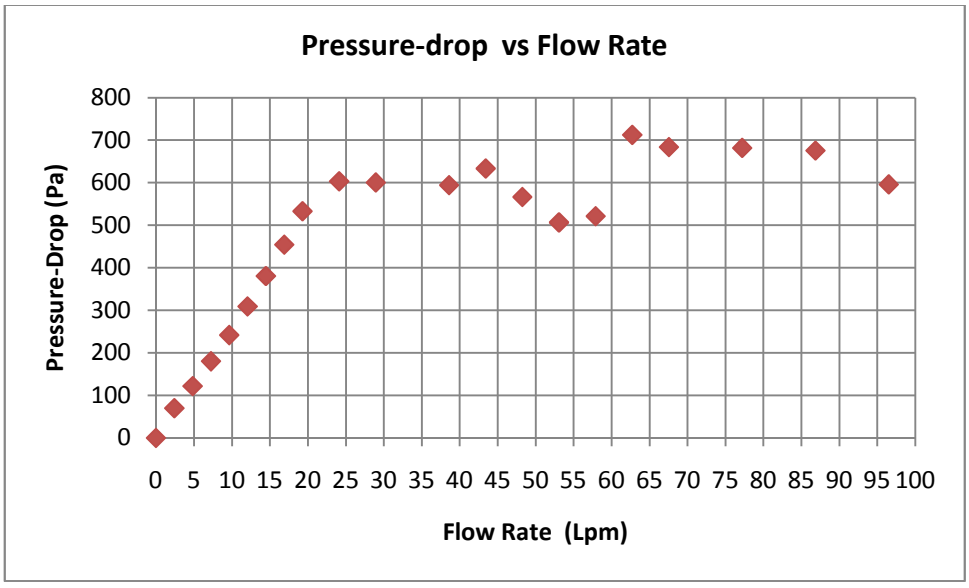

Figure 5.7: Coarse-Grid, Laminar Flow, Gidaspow-Drag Bed

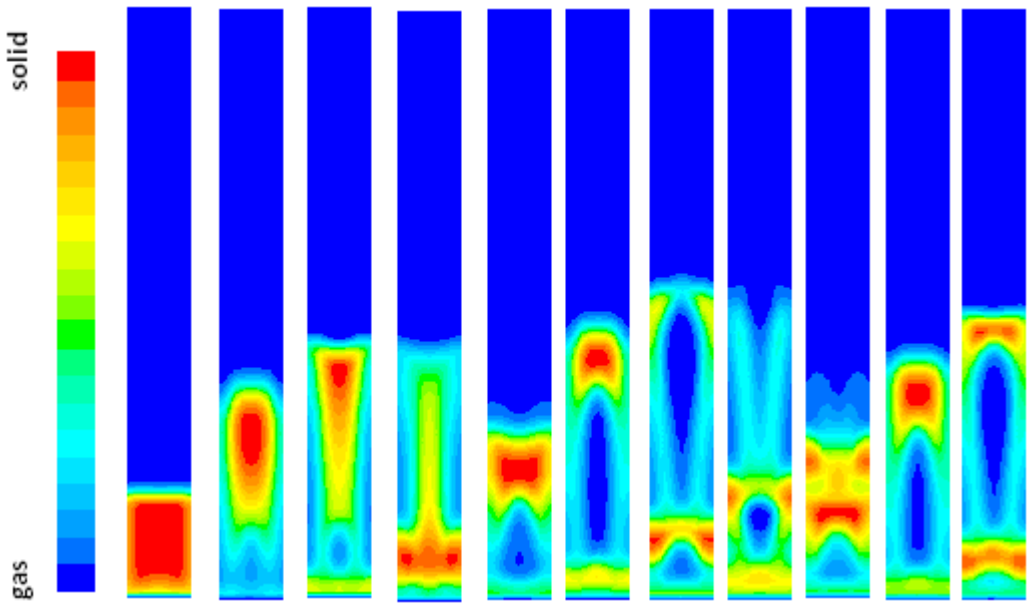

Figure 5.8: Contours of Solids Volume Fraction every 0.1 s for a Coarse-Grid, Laminar Flow, Gidaspow-Drag Bed at 200 cm/s

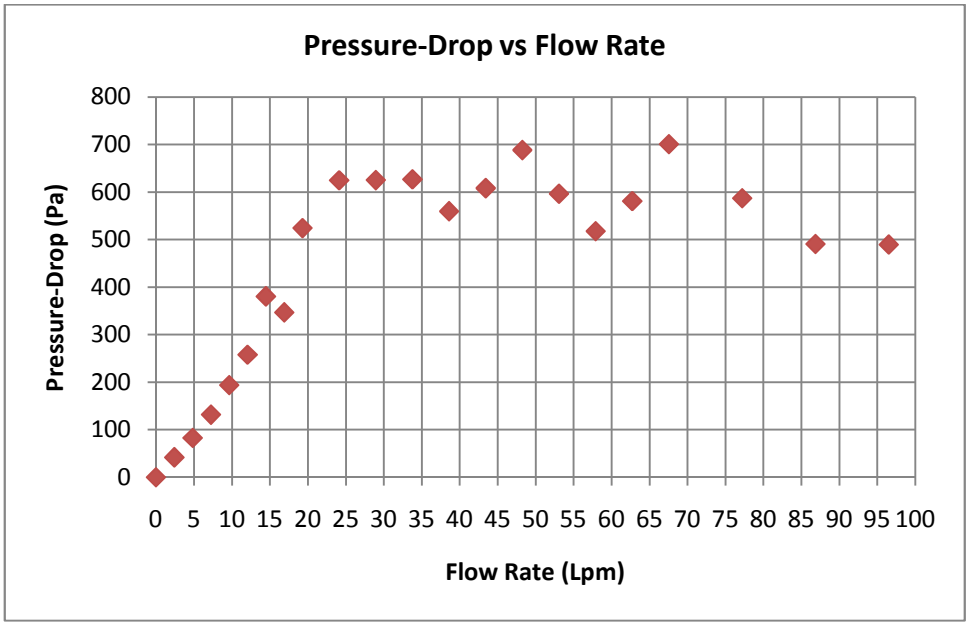

Figure 5.9: Coarse-Grid, Laminar Flow, Syamlal-Obrien-Drag Bed

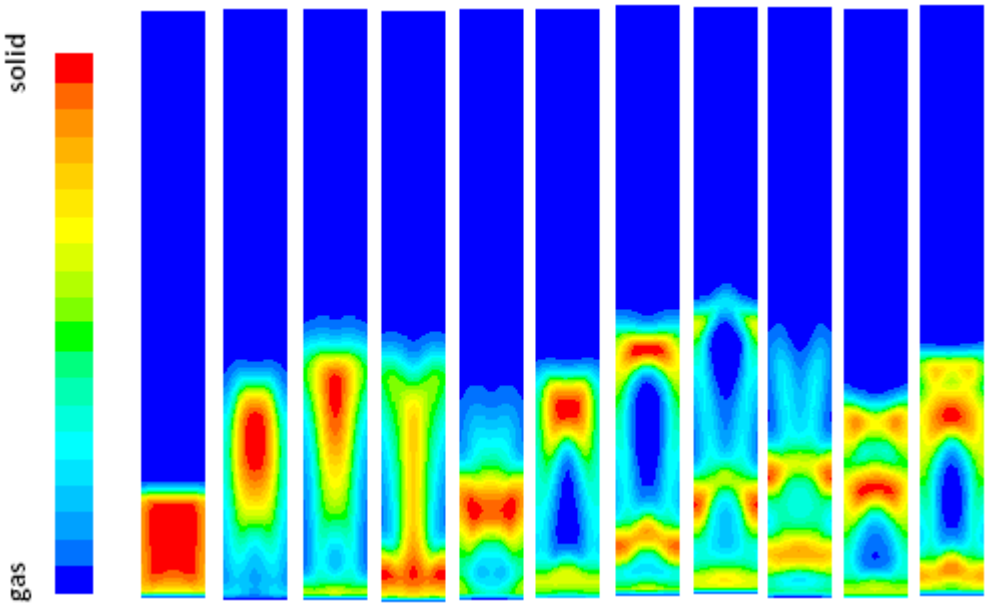

Figure 5.10: Contours of Solids Volume Fraction every 0.1 s for a Coarse-Grid, Laminar Flow, Syamlal-Obrien-Drag Bed at 200 cm/s

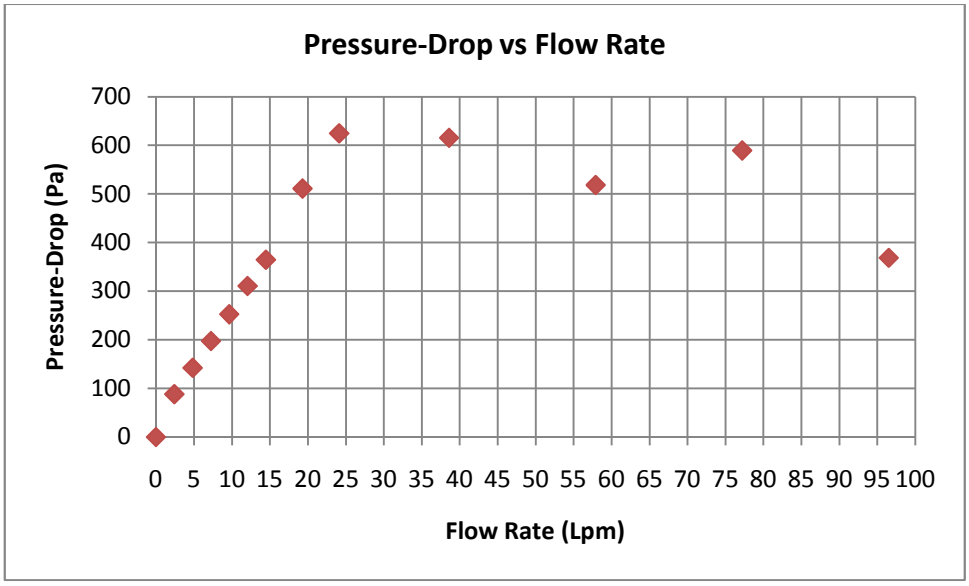

Figure 5.11: Coarse-Grid, Laminar Flow, Syamlal-Obrien Corrected-Drag Bed

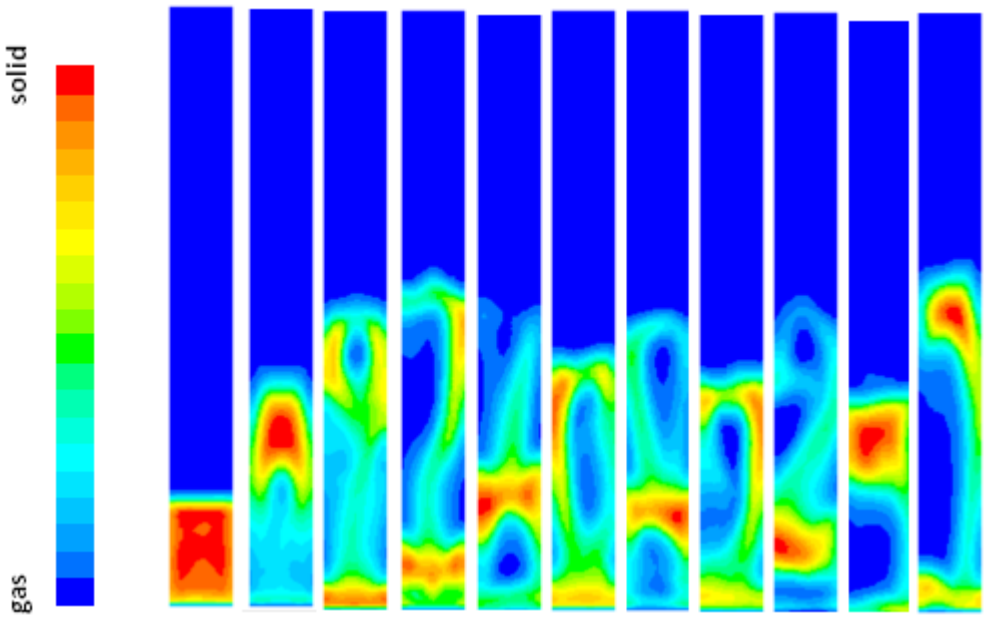

Figure 5.12: Contours of Solids Volume Fraction every 0.1 s for a Coarse-Grid, Laminar Flow, Syamlal-Obrien Corrected-Drag Bed at 200 cm/s

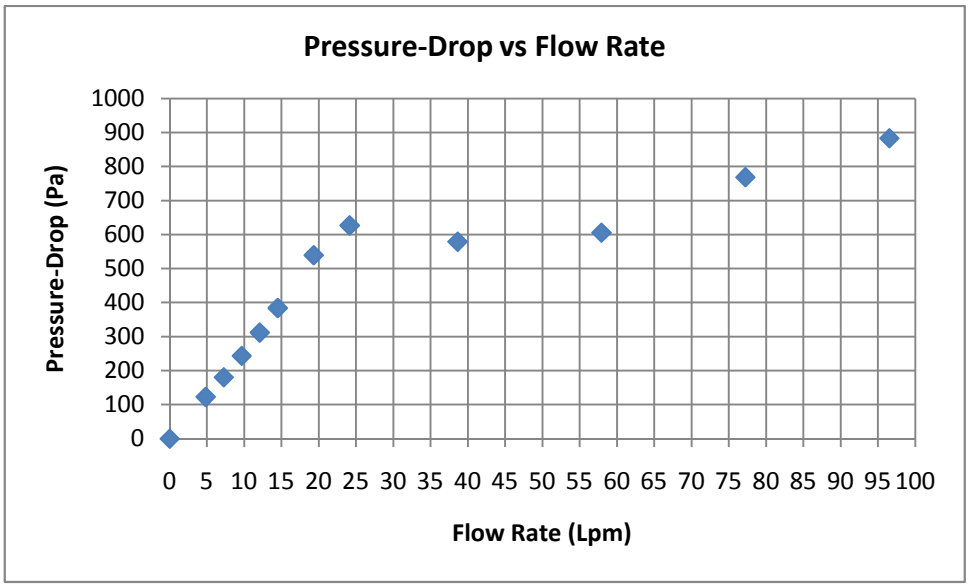

Figure 5.13: Coarse-Grid, Turbulent Flow, Gidaspow-Drag Bed

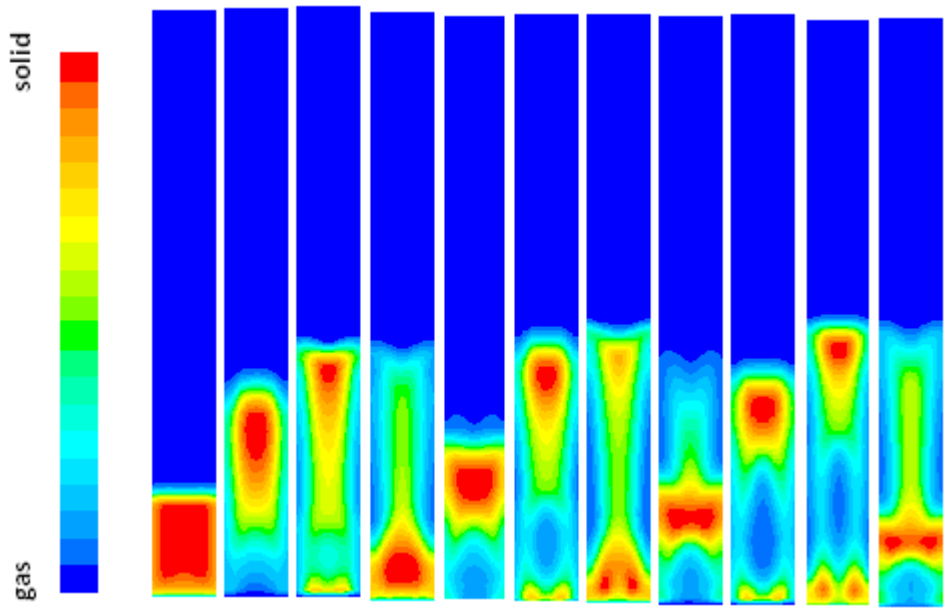

Figure 5.14: Contours of Solids Volume Fraction every 0.1 s for a Coarse-Grid, Turbulent Flow, Gidaspow-Drag Bed at 200 cm/s

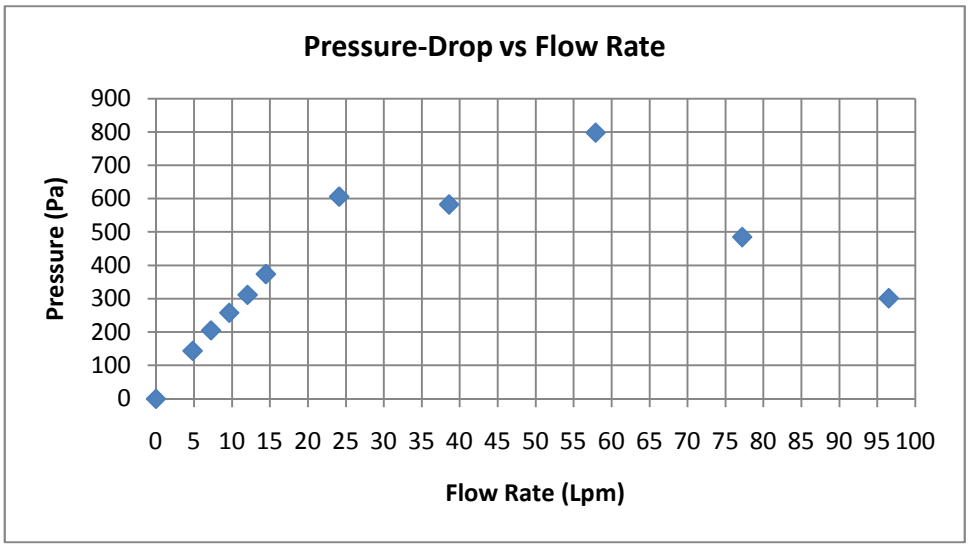

Figure 5.15: Coarse-Grid, Turbulent Flow, Syamlal-Obrien Corrected-Drag Bed

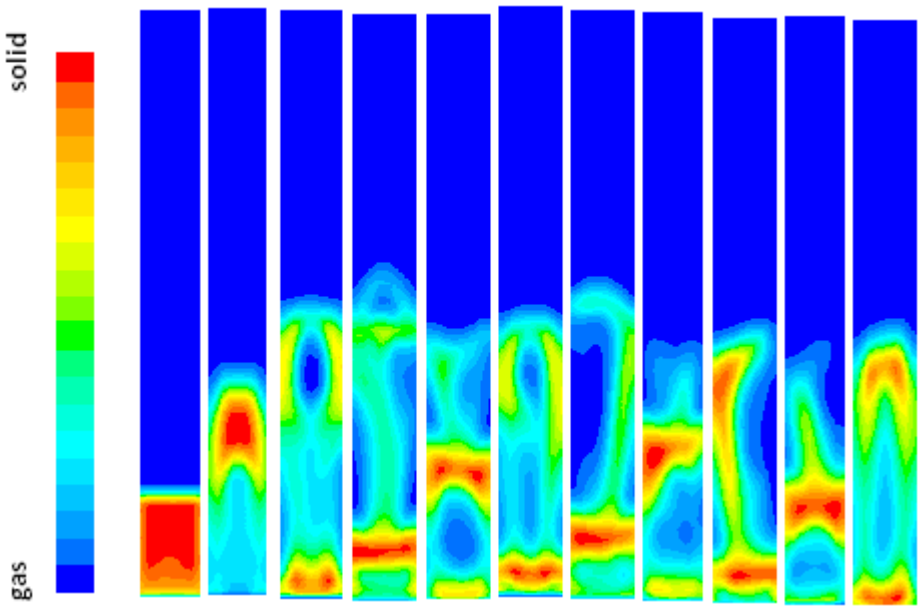

Figure 5.16: Contours of Solids Volume Fraction every 0.1 s for a Coarse-Grid, Turbulent Flow, Syamlal-Obrien Corrected-Drag Bed at 200 cm/s

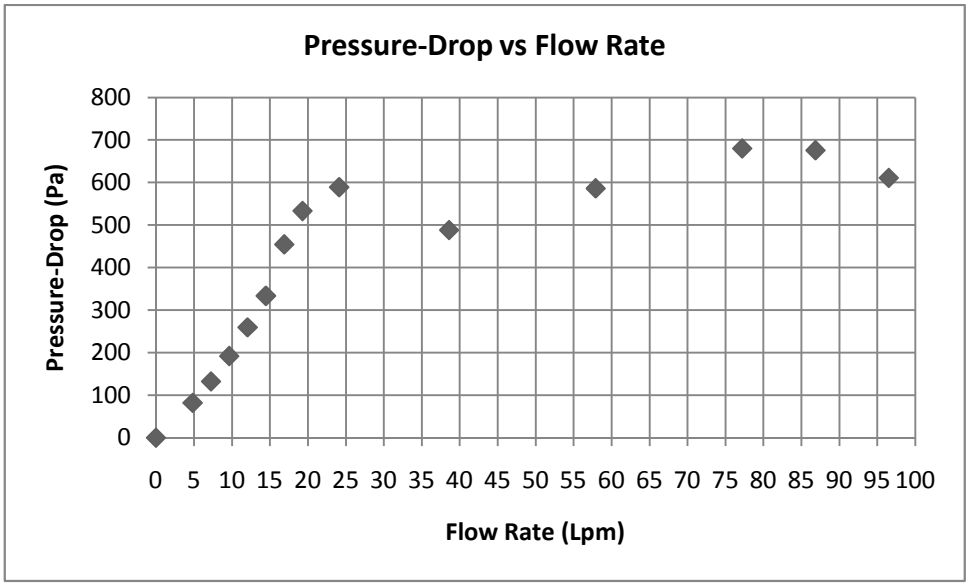

Figure 5.17: Fine-Grid, Laminar Flow, Syamlal-Obrien-Drag Bed

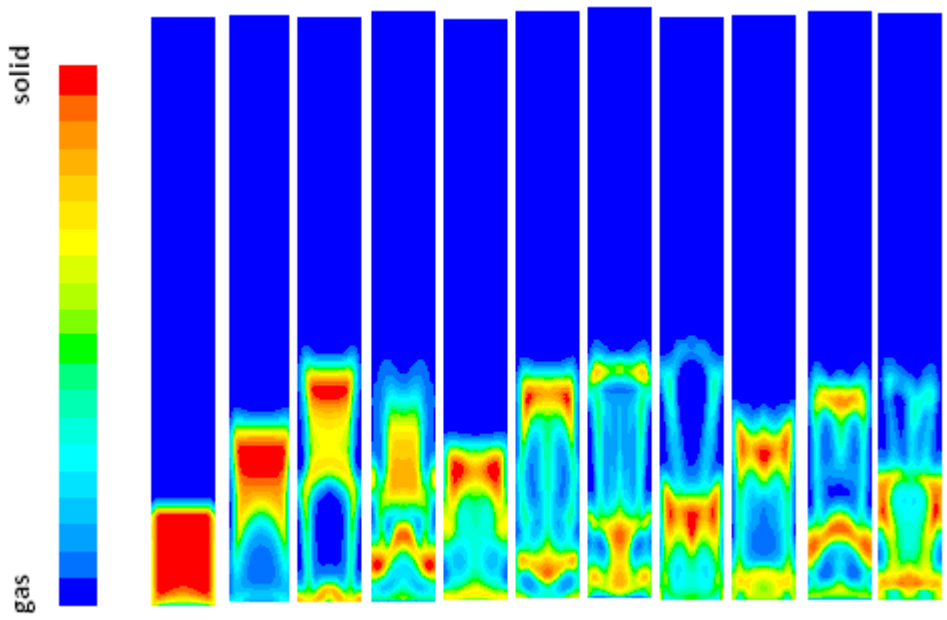

Figure 5.18: Contours of Solids Volume Fraction every 0.1 s for a Fine-Grid, Laminar Flow, Syamlal-Obrien-Drag Bed at 200 cm/s

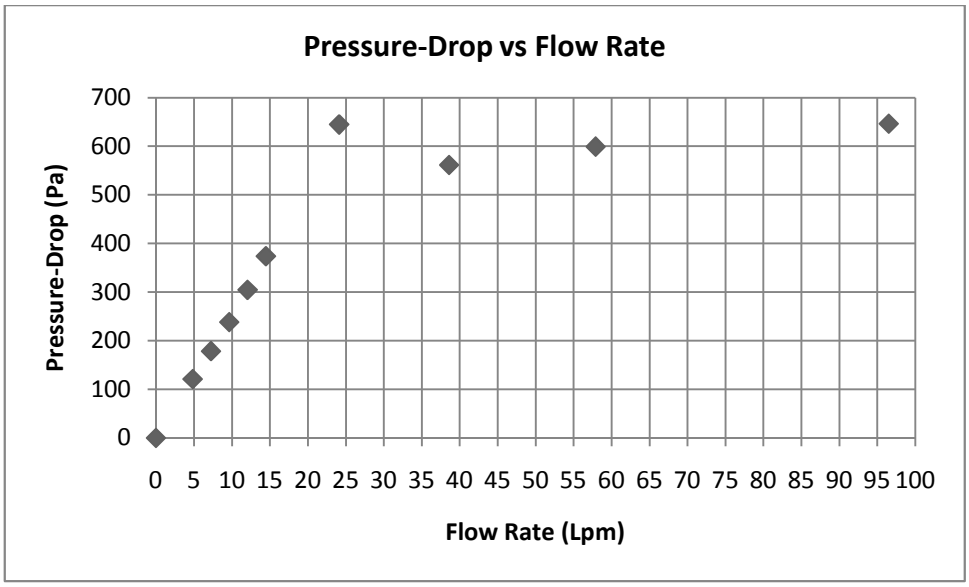

Figure 5.19: Fine-Grid, Laminar Flow, Gidaspow Bed

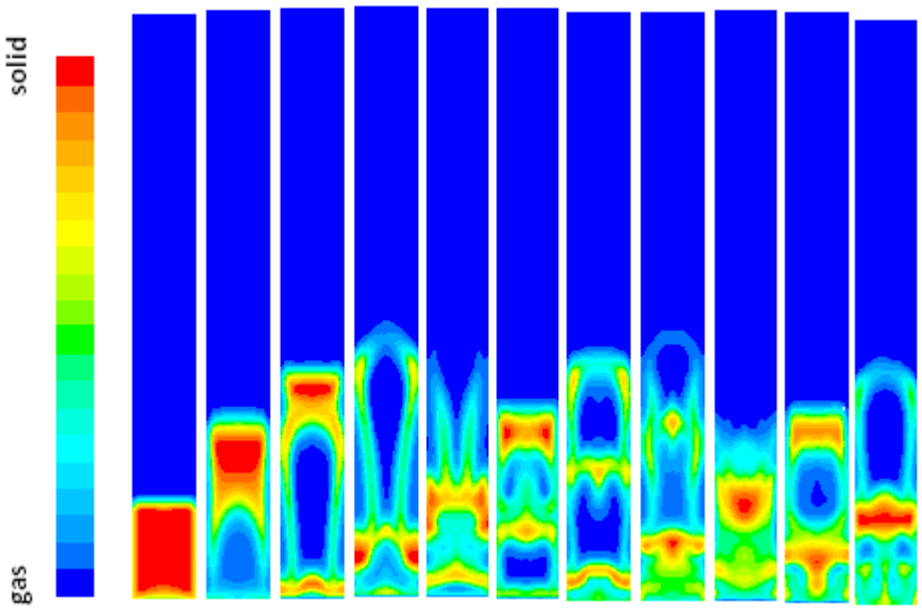

Figure 5.20: Contours of Solids Volume Fraction every 0.1 s for a Fine-Grid, Laminar Flow, Gidaspow Bed at 200 cm/s

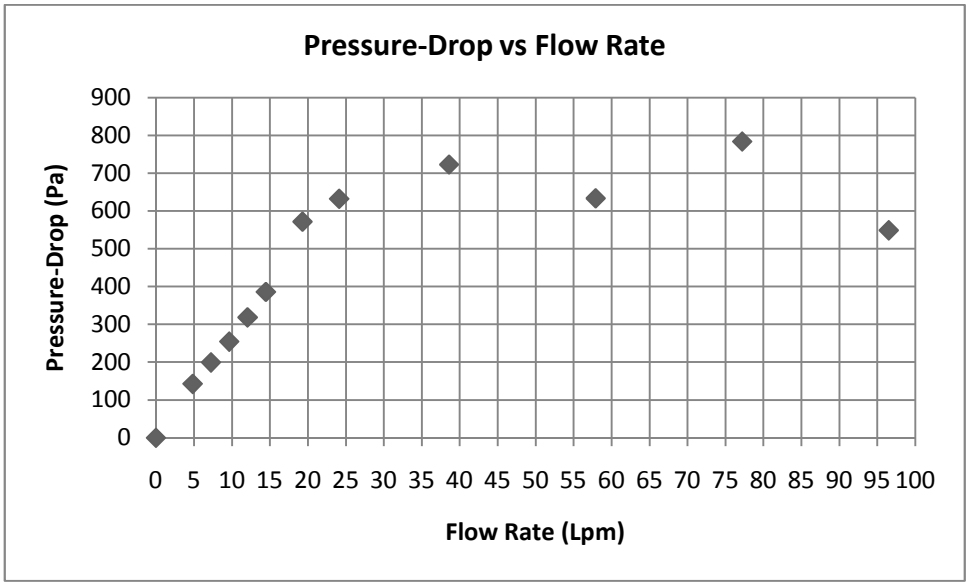

Figure 5.21: Fine-Grid, Laminar Flow, Syamlal-Obrien Corrected Bed

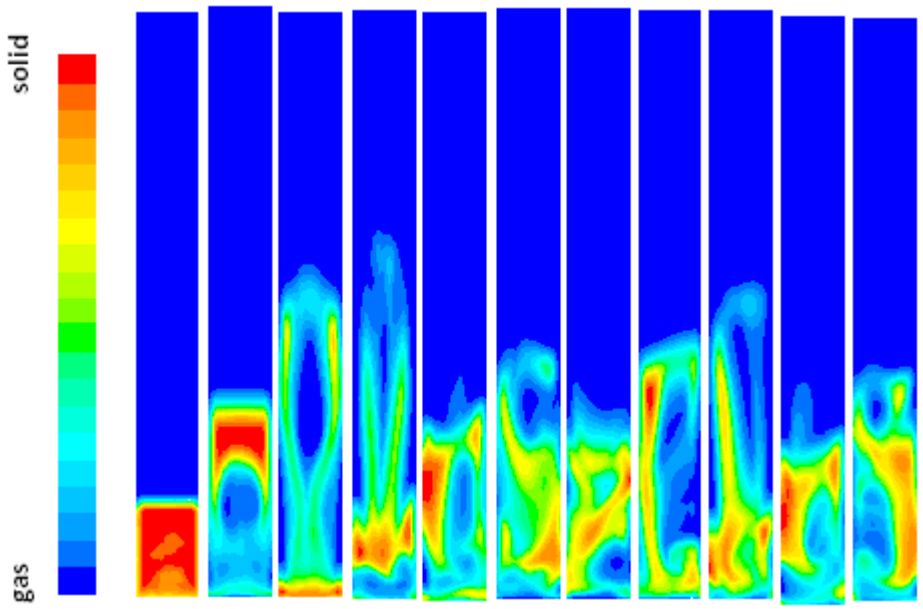

Figure 5.22: Contours of Solids Volume Fraction every 0.1 s for a Fine-Grid, Laminar Flow, Syamlal-Obrien Corrected Bed at 200 cm/s

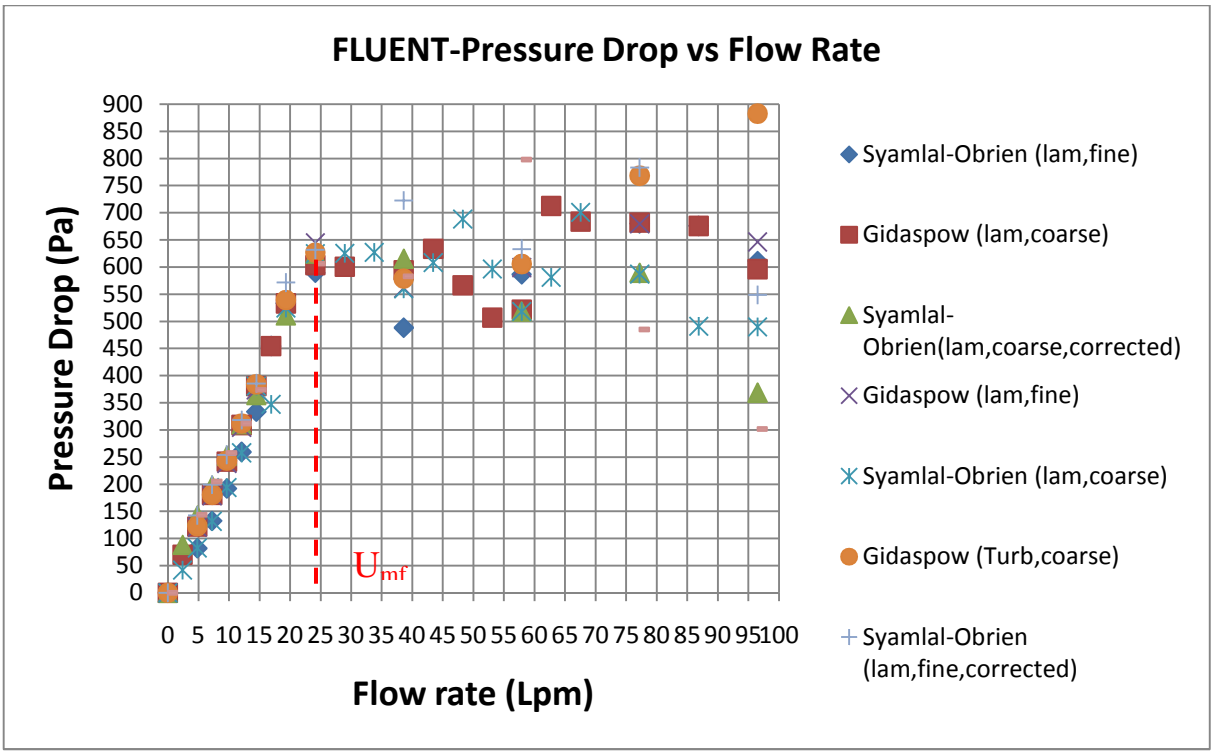

Figure 5.23: All Fluent Fluidization Results

5.5.2 MFIX Code Results

The following values were obtained by MFIX in order to design the fluidization curves. Each interaction of flow factors is shown in the next charts. The run time was for 1 second with a time-step of 0.001 s.

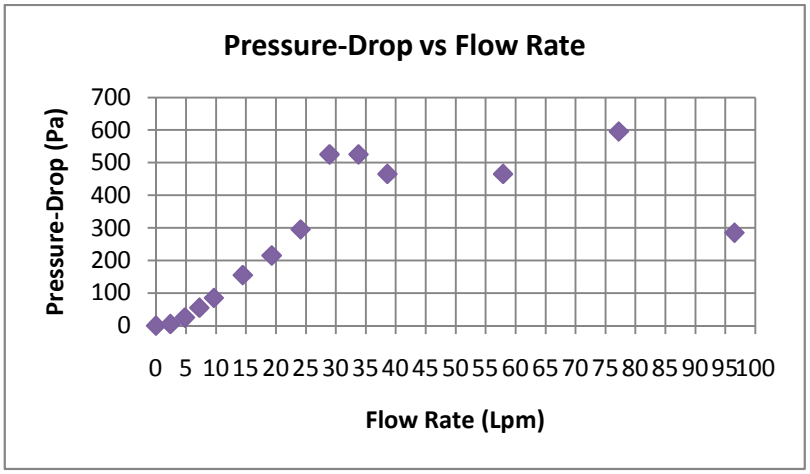

Figure 5.24: First Order, Laminar Flow, Gidaspow-Drag Bed

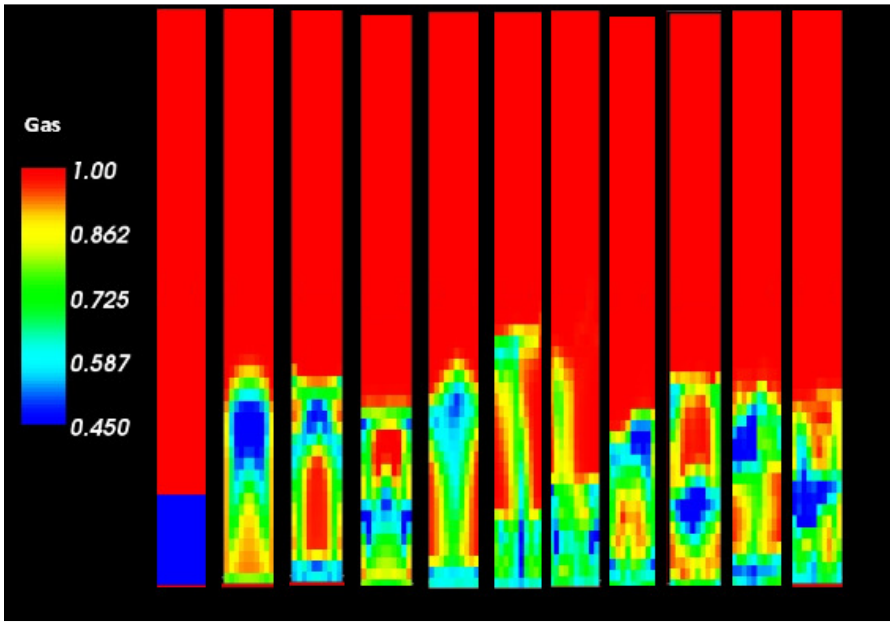

Figure 5.25: Contours of Gas Volume Fraction every 0.1 s for a First Order, Laminar Flow, Gidaspow-Drag Bed at 200 cm/s

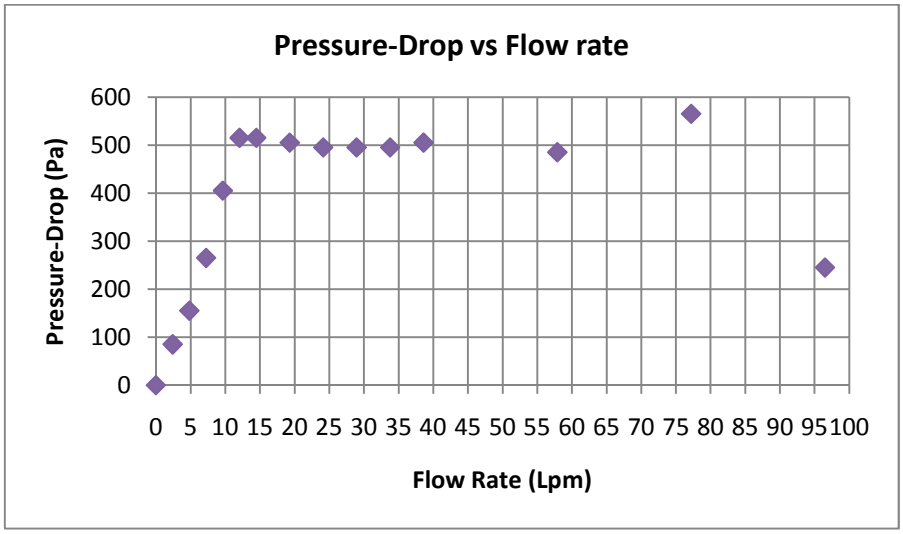

Figure 5.26: First Order, Laminar Flow, Syamlal-Obrien Corrected-Drag Bed

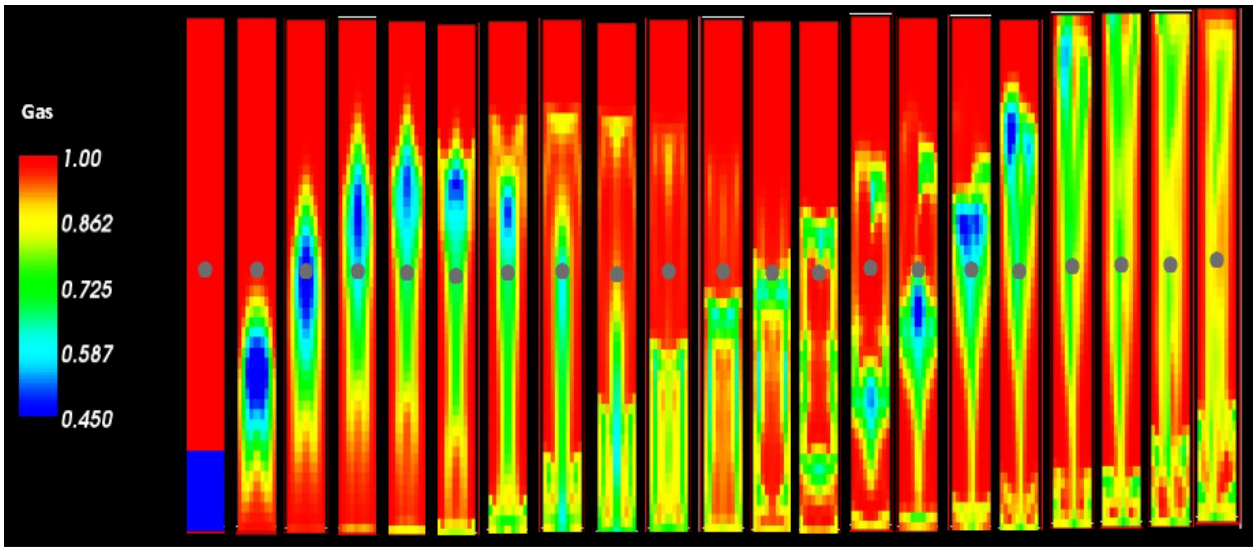

Figure 5.27: Contours of Gas Volume Fraction every 0.1 s for a First Order, Laminar Flow, Syamlal-Obrien Corrected-Drag Bed at 200 cm/s

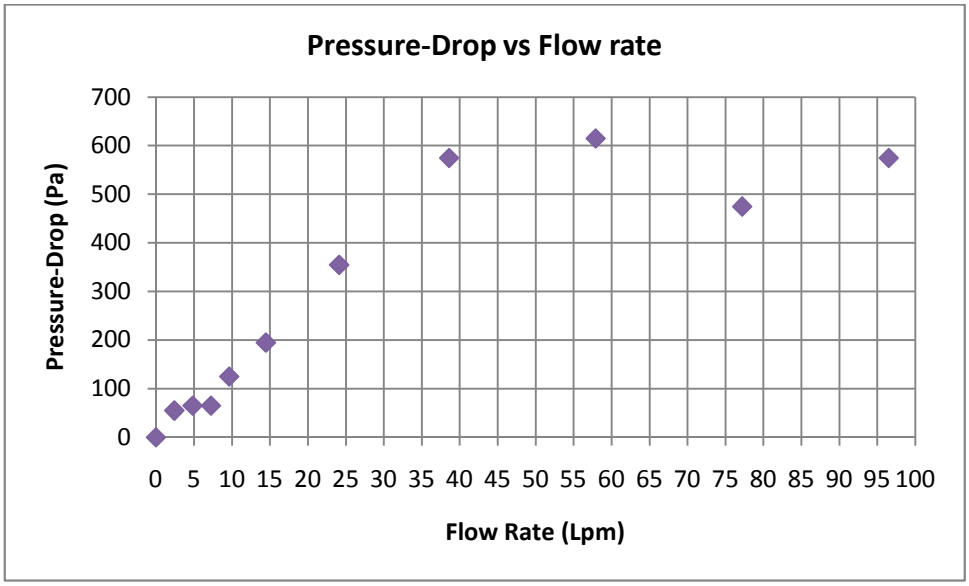

Figure 5.28: Second Order, Laminar Flow, Gidaspow-Drag Bed

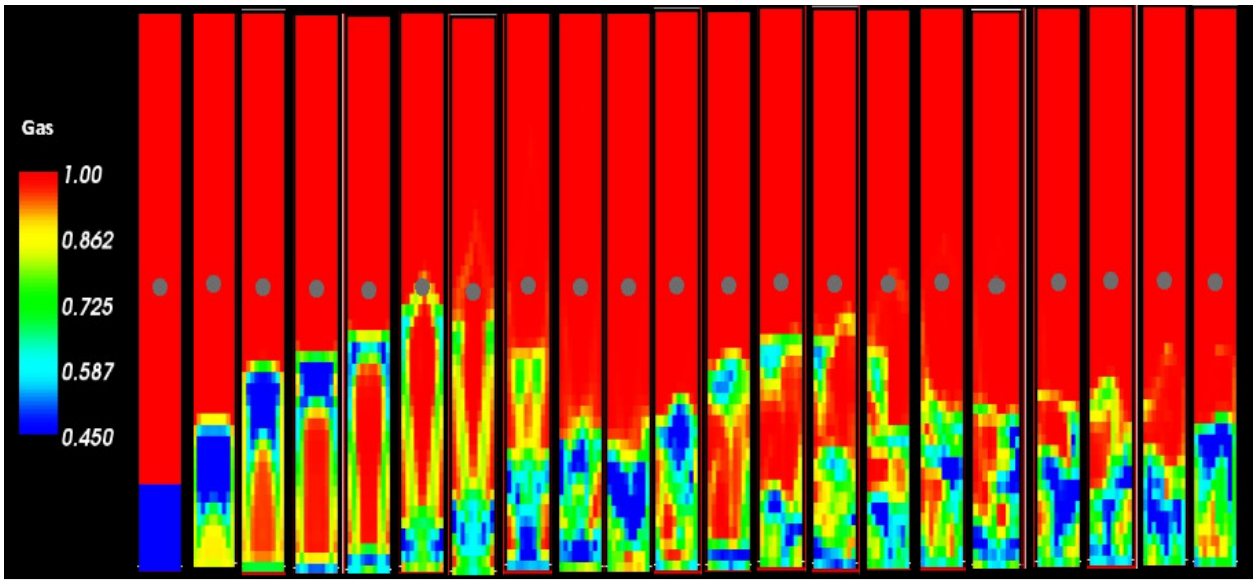

Figure 5.29: Contours of Gas Volume Fraction every 0.1 s for a Second Order, Laminar Flow, Gidaspow-Drag Bed at 200 cm/s

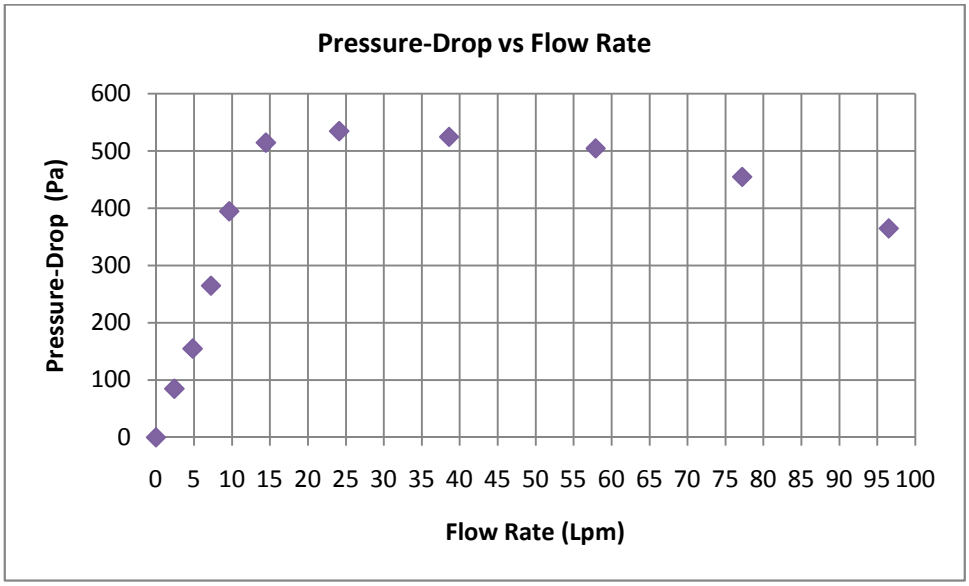

Figure 5.30: Second Order, Laminar Flow, Syamlal-Obrien Corrected-Drag Bed

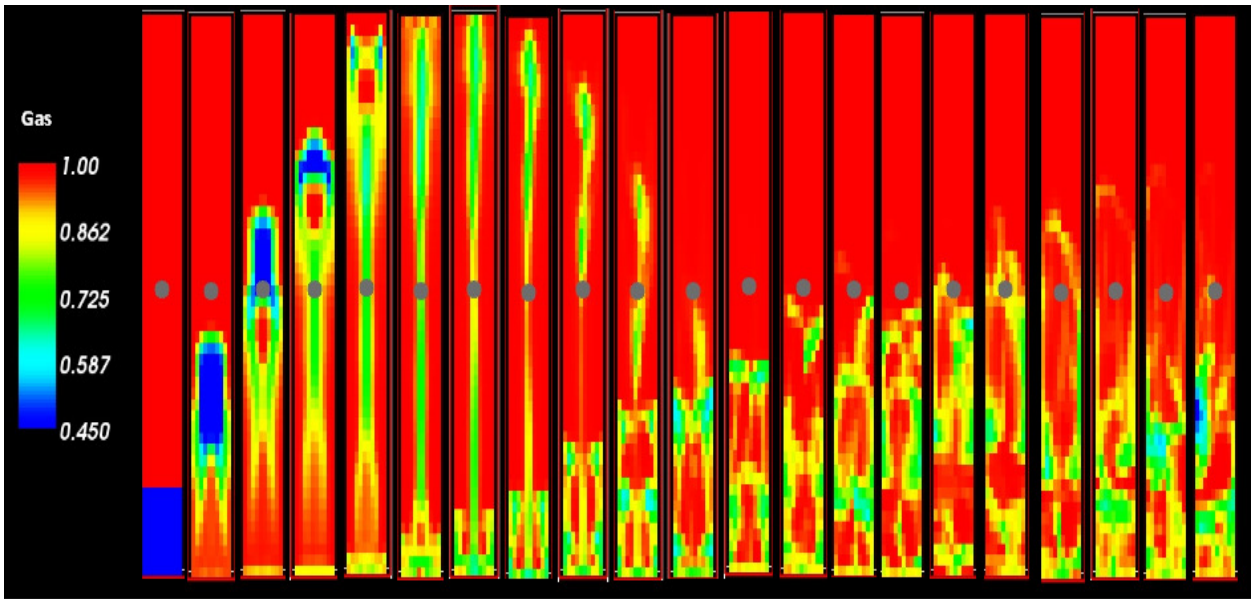

Figure 5.31: Contours of Gas Volume Fraction every 0.1 s for a Second Order, Laminar Flow, Syamlal-Obrien Corrected-Drag Bed at 200 cm/s

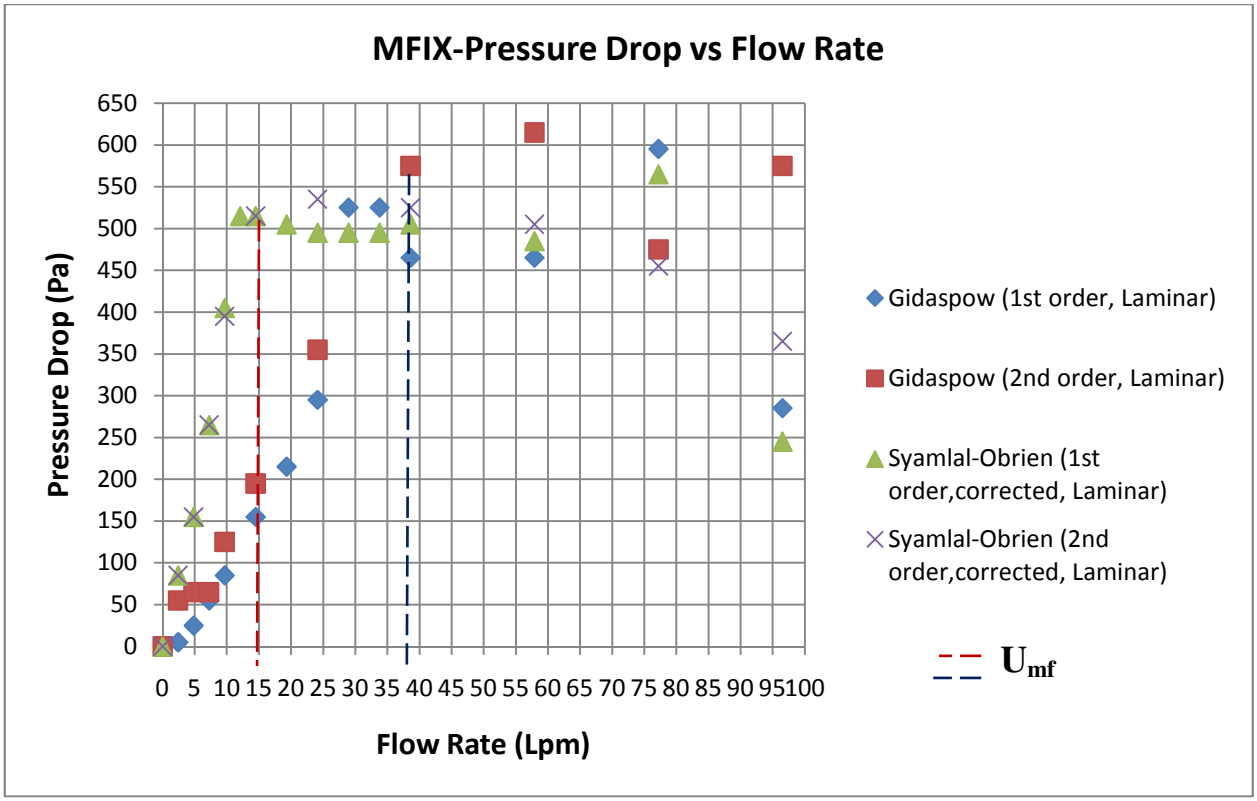

Figure 5.32: All MFIX Fluidization Results

5.6 Theoretical Comparison

By using the following theoretical correlations for Reynolds number at minimum fluidization based on the pressure drop principles, the minimum fluidization can be calculated and compare with those found on the simulations.

Correlation: $Re_{mf} = (A_1^2 + B_1 Ar)^{1/2} - A_1$, $\alpha = (1-\epsilon)/\phi_s^2 \epsilon^3$, $\beta = 1/(\phi_s \epsilon^3)$, $m = \alpha/\beta$

Ref.	Constants		
	A_1	B_1	m
Ergun[42]	$42.85/\alpha$	$0.57/\beta$	$(1-\epsilon)/\phi_s$
Wen and Yu[33]	33.7	0.0408	0.7857

Therefore, the following table was developed:

Table 4: Results Comparison: Theoretical and Simulation

Correlation	Minimum Fluidization Velocity (cm/s)	Flow Rate (Lpm)
Ergun	68.06	32.84
Wen and yu	48.96	23.63
Fluent	51.81	25.00
MFIX (Syamlal-Obrien)	78.75	38.00
MFIX (Gidaspow)	31.08	15.00

5.7 Experimental Comparison

Running a fluidized bed experiment of the same characteristics as the computational analysis was performed showing the following results:

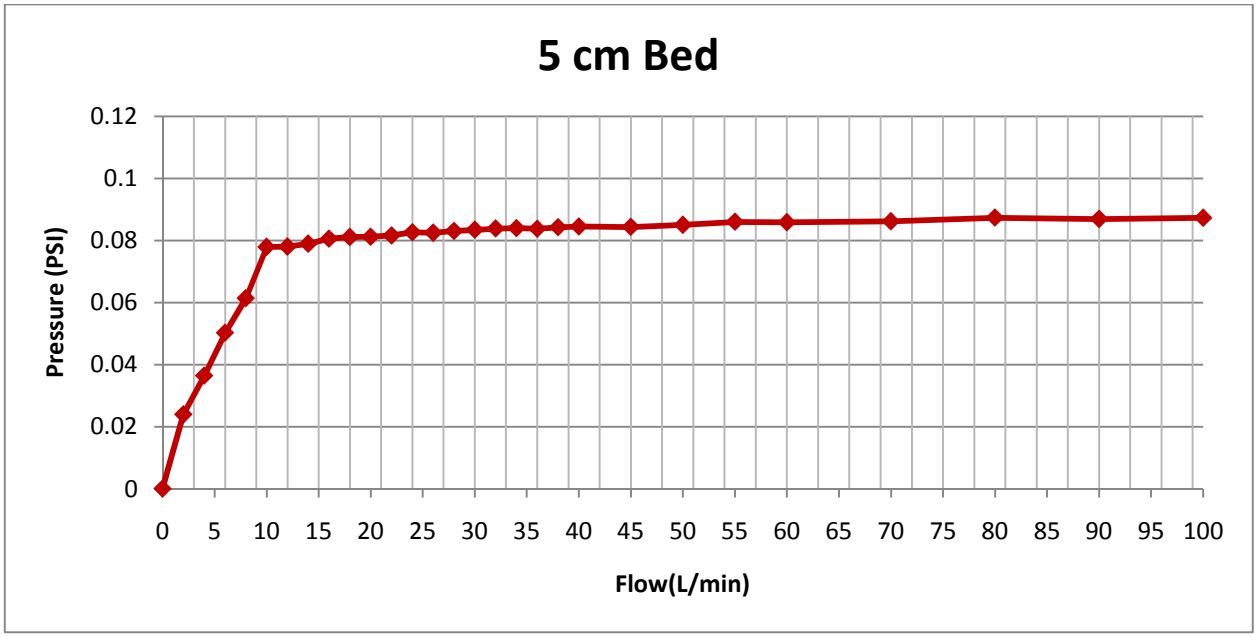

Figure 5.33: Experimental Results for Fluidized Bed Experiment

Where the pressure stabilizes at ~0.078 PSI which is around 538 Pa. Table 5 shows the comparison with the computational analysis

Table 5: Results Comparison: Experimental and Simulation

Correlation	Minimum Fluidization Velocity (cm/s)	Flow Rate (Lpm)
Experimental	21.00	10.00
Fluent	51.81	25.00
MFIX (Syamlal-Obrien)	78.75	38.00
MFIX (Gidaspow)	31.08	15.00

CHAPTER 6: FLUIDIZED BED SIMULATION

6.1 Conclusions

The present thesis has addressed the simulation of a gas-solid fluidized bed by conducted an Eulerian-Eulerian approach for both fluid and solid phase. Two computational codes were utilized to carry out the aforementioned simulations, these being Fluent CFD code and MFIX code. In addition the effect of various drag correlations on the bed simulations was studied. Simulation of laminar and turbulent flow was also performed. According to the results obtained in Table 4, it can be appreciated that some variations exist between Fluent Code and MFIX Code. Moreover, the validation with the physical experiment shows variation also as appreciated in Table 5. However the Fluent simulation shows consistency in all the runs compared to MFIX. This investigation aims to contribute to future understanding in fluidized bed technologies.

6.2 Recommendations

In order to improve the results finer grids could be generated; in addition the use of the Discrete Element Model (DEM) could improve the accuracy of the results. In DEM the fluid phase is analyzed using Eulerian approach while the motion of individual particle is tracked using Newton's laws, accounting for collision dynamics between particles, also including walls forces and the solid-fluid interaction forces. This approach to analyze the solid phase is known as Lagrangian approach. Other effects such as heat and mass transfer can be taken into consideration with this Eulerian-Lagrangian approach for better understanding of fluidized beds.

REFERENCES

[1] Wu, W.Y.. "Hydrodynamic characteristics of a magnetically stabilized air fluidized bed of an admixture of magnetic and non-magnetic particles", Powder Technology.

[2] Geldart, D. Types of gas fluidization, Powder Technology, 7, 285-292, (1973).

[3] Rahul Dixit. "Fluidization technologies: Aerodynamic principles and process engineering", Journal of Pharmaceutical Sciences, 2009.

[4] B. J. Glasser. "From Bubbles to Clusters in Fluidized Beds", Physical Review Letters, 08/1998

[5] Geldart, D., Powder Technol., 7, 285, 1973.

[6] C.K. Gupta, D. Sathiyamoorthy., Fluid bed technology in materials processing, CRC Press, 1999.

[7] Hugo A. Jakobsen. "Fluidized Bed Reactors", Chemical Reactor Modeling, 2008.

[8] Li, S.. "Modelling of the behaviour of gas-solid two-phase mixtures flowing through packed beds", Chemical Engineering Science, 200603.

[9] Johri, J.. "A bifurcation approach to understanding instabilities in gas-fluidized beds using a single phase compressible flow model", Computers and Chemical Engineering, 20041115.

[10] Detamore, M.S.. "A kinetic-theory analysis of the scale-up of circulating fluidized beds", Powder Technology, 20010523.

[11] M. Syamlal, W. Rogers, and O'Brien T. J. MFIX Documentation: Volume 1, Theory Guide. National Technical Information Service, Springfield, VA, 1993. DOE/METC-9411004, NTIS/DE9400087.

[12] J. R. Howard, Fluidized Bed Technology: principles and applications, Adam Hilger; Adam Hilger, Bristol and New York, J R Howard 1989.

[13] T. B. Anderson and R. Jackson. A Fluid Mechanical Description of Fluidized Beds. I & EC Fundam., 1967.

[14] M. Syamlal and T. J. O'Brien. Computer Simulation of Bubbles in a Fluidized Bed. AIChE Symp. Series, 85:22–31, 1989.

[15] J. M. Dalla Valle. Micromeritics. Pitman, London, 1948.

[16] M. Syamlal. The Particle-Particle Drag Term in a Multiparticle Model of Fluidization. National Technical Information Service, Springfield, VA, 1987. DOE/MC/21353-2373, NTIS/DE87006500.

[17] J. R. Richardson and W. N. Zaki. Sedimentation and Fluidization: Part I. Trans. Inst. Chem. Eng., 32:35–53, 1954.

[18] D. Gidaspow, R. Bezburuah, and J. Ding. Hydrodynamics of Circulating Fluidized Beds, Kinetic Theory Approach. In Fluidization VII, Proceedings of the 7th Engineering Foundation Conference on Fluidization, pages 75–82, 1992.

[19] S. Ogawa, A. Umemura, and N. Oshima. On the Equation of Fully Fluidized Granular Materials. J. Appl. Math. Phys., 31:483, 1980.

[20] T.-H. Shih, W. W. Liou, A. Shabbir, Z. Yang, and J. Zhu. A New k-_ Eddy-Viscosity Model for High Reynolds Number Turbulent Flows - Model Development and Validation. Computers Fluids, 24(3):227–238, 1995.

[21] Crowe C., Sommerfeld M., and Tsuji Y., 1998, Multiphase flows with dropletsand particles, CRC Press, New York

APPENDIX

Table 6: Coarse-Grid, Laminar Flow, Gidaspow-Drag Bed

V-inlet (cm/s)	Flow-inlet (Lpm)	Pressure-drop (Pa)
0	0	0
5	2.41	69.95
10	4.83	121.92
15	7.24	180.19
20	9.65	241.77
25	12.06	309.08
30	14.48	380.62
35	16.89	454.45
40	19.30	533.02
50	24.13	603.49
60	28.95	600.54
80	38.60	594.25
90	43.43	633.44
100	48.25	566.42
110	53.08	506.7
120	57.91	521.4
130	62.73	712.38
140	67.56	683.84
160	77.21	681.86
180	86.86	675.63
200	96.51	596.04

Table 7: Coarse-Grid, Laminar Flow, Syamlal-Obrien-Drag Bed

V-inlet (cm/s)	Flow-inlet (Lpm)	Pressure-drop (Pa)
0	0	0
5	2.41	41.85
10	4.83	82.58
15	7.24	131.63
20	9.65	193.87
25	12.06	257.79
30	14.48	380.62
35	16.89	346.92
40	19.30	524.33
50	24.13	624.81
60	28.95	625.26
70	33.78	626.99
80	38.60	559.74
90	43.43	608.39
100	48.25	688.41
110	53.08	596.45
120	57.91	517.85
130	62.73	581.05
140	67.56	700.82
160	77.21	587.07
180	86.86	490.92
200	96.51	489.62

Table 8: Coarse-Grid, Laminar Flow, Syamlal-Obrien Corrected-Drag Bed

V-inlet (cm/s)	Flow-inlet (Lpm)	Pressure-drop (Pa)
0	0	0
5	2.41	88.16
10	4.83	142.26
15	7.24	197.48
20	9.65	252.5
25	12.06	310.57
30	14.48	364.54
40	19.30	511.07
50	24.13	624.62
80	38.60	615.42
120	57.91	518.41
160	77.21	589.54
200	96.51	368.61

Table 9: Coarse-Grid, Turbulent Flow, Gidaspow-Drag Bed

V-inlet (cm/s)	Flow-inlet (Lpm)	Pressure-drop (Pa)
0	0	0
10	4.83	122.78
15	7.24	180.54
20	9.65	243.26
25	12.06	311.82
30	14.48	383.98
40	19.30	539.13
50	24.13	626.67
80	38.60	578.8
120	57.91	605.57
160	77.21	768.33
200	96.51	882.67

Table 10: Coarse-Grid, Turbulent Flow, Syamlal-Obrien Corrected-Drag Bed

V-inlet (cm/s)	Flow-inlet (Lpm)	Pressure-drop (Pa)
0	0	0
10	4.83	143.95
15	7.24	205.19
20	9.65	257.8
25	12.06	311.64
30	14.48	373.96
50	24.13	606.19
80	38.60	582.67
120	57.91	798.02
160	77.21	485.05
200	96.51	301.68

Table 11: Fine-Grid, Laminar Flow, Syamlal-Obrien-Drag Bed

V-inlet (cm/s)	Flow-inlet (Lpm)	Pressure-drop (Pa)
0	0	0
10	4.83	81.98
15	7.24	132.34
20	9.65	191.96
25	12.06	259.4
30	14.48	333.5
35	16.89	454.45
40	19.30	533.02
50	24.13	589.09
80	38.60	488.08
120	57.91	586.15
160	77.21	679.85
180	86.86	675.63
200	96.51	610.8

Table 12: Fine-Grid, Laminar Flow, Gidaspow-Drag Bed

V-inlet (cm/s)	Flow-inlet (Lpm)	Pressure-drop (Pa)
0	0	0
10	4.83	120.88
15	7.24	178.42
20	9.65	238.24
25	12.06	304.52
30	14.48	373.87
50	24.13	644.8
80	38.60	561.33
120	57.91	599.14
160	77.21	679.5
200	96.51	646.2

Table 13: Fine-Grid, Laminar Flow, Syamlal-Obrien Corrected-Drag Bed

V-inlet (cm/s)	Flow-inlet (Lpm)	Pressure-drop (Pa)
0	0	0
10	4.83	142.6
15	7.24	199.25
20	9.65	254.24
25	12.06	318.41
30	14.48	385.71
40	19.30	571.43
50	24.13	631.8
80	38.60	722.48
120	57.91	633.23
160	77.21	783.27
200	96.51	548.69

Table 14: First order, Laminar Flow, Gidaspow-Drag Bed

V-inlet (cm/s)	Flow-inlet (Lpm)	Pressure-drop (Pa)
0	0	0
5	2.41	5
10	4.83	25
15	7.24	55
20	9.65	85
30	14.48	155
40	19.30	215
50	24.13	295
60	28.95	525
70	33.78	525
80	38.60	465
120	57.91	465
160	77.21	595
200	96.51	285

Table 15: First order, Laminar Flow, Syamlal-Obrien Corrected-Drag Bed

V-inlet (cm/s)	Flow-inlet (Lpm)	Pressure-drop (Pa)
0	0	0
5	2.41	85
10	4.83	155
15	7.24	265
20	9.65	405
25	12.06	515
30	14.48	515
40	19.30	505
50	24.13	495
60	28.95	495
70	33.78	495
80	38.60	505
120	57.91	485
160	77.21	565
200	96.51	245

Table 16: Second order, Laminar Flow, Gidaspow-Drag Bed

V-inlet (cm/s)	Flow-inlet (Lpm)	Pressure-drop (Pa)
0	0	0
5	2.41	55
10	4.83	65
15	7.24	65
20	9.65	125
30	14.48	195
50	24.13	355
80	38.60	575
120	57.91	615
160	77.21	475
200	96.51	575

Table 17: Second order, Laminar Flow, Syamlal-Obrien Corrected-Drag Bed

V-inlet (cm/s)	Flow-inlet (Lpm)	Pressure-drop (Pa)
0	0	0
5	2.41	85
10	4.83	155
15	7.24	265
20	9.65	395
30	14.48	515
50	24.13	535
80	38.60	525
120	57.91	505
160	77.21	455
200	96.51	365

Table 18: User Defined Function for Syamlal-Obrien Corrected Drag Correlation

```
/* This is a routine for customizing default Syamlal drag law in Fluent 6.3
   The default drag law uses 0.8 (for void<=0.85) and 2.65 (void>0.85) for
   bfac. This is for a min fluid vel of 70 cm/s. The current drag law has been
   tuned for a min fluid vel of 20 cm/s and uses 0.26 and 9.56872 for these
   parameters. */

#include "udf.h"
#include "sg_mphase.h"

# define pi 4.*atan(1.)
#define diam2 1.e-3

DEFINE_EXCHANGE_PROPERTY(custom_drag_syam, cell, mix_thread, s_col, f_col)
{
 Thread *thread_g, *thread_s;
 real x_vel_g, x_vel_s, y_vel_g, y_vel_s, abs_v, slip_x, slip_y,
      rho_g, rho_s, mu_g, reyp, afac,
      bfac, void_g, vfac, fdrgs, taup, k_g_s;

 /* find the threads for the gas (primary) and solids (secondary phases).
These phases appear in columns 2 and 1 in the Interphase panel respectively*/

 thread_g = THREAD_SUB_THREAD(mix_thread, s_col);/*gas phase*/
 thread_s = THREAD_SUB_THREAD(mix_thread, f_col);/* solid phase*/

 /* find phase velocities and properties*/

 x_vel_g = C_U(cell, thread_g);
 y_vel_g = C_V(cell, thread_g);

 x_vel_s = C_U(cell, thread_s);
 y_vel_s = C_V(cell, thread_s);

 slip_x = x_vel_g - x_vel_s;
 slip_y = y_vel_g - y_vel_s;

 rho_g = C_R(cell, thread_g);
 rho_s = C_R(cell, thread_s);

 mu_g = C_MU_L(cell, thread_g);

 /*compute slip*/
 abs_v = sqrt(slip_x*slip_x + slip_y*slip_y);

 /*compute reynolds number*/

 reyp = rho_g*abs_v*diam2/mu_g;

 /* compute particle relaxation time */

 taup = rho_s*diam2*diam2/18./mu_g;

 void_g = C_VOF(cell, thread_g);/* gas vol frac*/

 /*compute drag and return drag coeff, k_g_s*/
```

```
 afac = pow(void_g,4.14);

 if(void_g<=0.85)
  bfac = 0.26*pow(void_g, 1.28);
 else
  bfac = pow(void_g, 9.56872);

 vfac = 0.5*(afac-0.06*reyp+sqrt(0.0036*reyp*reyp+0.12*reyp*(2.*bfac-
              afac)+afac*afac));
 fdrgs = void_g*(pow((0.63*sqrt(reyp)/vfac+4.8*sqrt(vfac)/vfac),2))/24.0;

 k_g_s = (1.-void_g)*rho_s*fdrgs/taup;


 return k_g_s;
```

Table 19: MFIX DAT File Example

```
#
#  Fluidized Bed Simulation
#
#  Mario A. Ruvalcaba          11-05-09
#
# Run time for F90 allocatable arrays on Octane -- 3.3 h
# Run-control section
#
  RUN_NAME = 'CM-L-SO'
  DESCRIPTION = 'Fluidized Bed Simulation'
  RUN_TYPE = 'new'
  UNITS = 'cgs'
  TIME  = 0.0    TSTOP = 1.0    DT = 1.0E-3    DT_MIN = 1.0E-12
  NORM_G = 0.0d0    NORM_S = 0.0d0    MAX_NIT = 30
  DISCRETIZE = 9*2
  ENERGY_EQ = .FALSE.
  SPECIES_EQ = .FALSE.    .FALSE.
#
# Physical Parameters
#
  UR_FAC(1) = 0.5

#
# Geometry Section
#
  COORDINATES = 'cylindrical'

  XLENGTH  =  1.6    IMAX =   6
  YLENGTH  =  30     JMAX =   50
  ZLENGTH  = @(2*Pi) KMAX =   8



#
# Gas-phase Section
#
```

```
  MU_g0 = 1.8E-4
  MW_avg = 29.
#
# Solids-phase Section
#
  DRAG_TYPE = 'SYAM_OBRIEN'
  Drag_c1 = 0.26
  Drag_d1 = 9.56872
  RO_s    = 2.23
  D_p0    = 0.1

  e       = 0.8
  Phi     = 0.0
  EP_star = 0.45
#
# Initial Conditions Section
#
       !              Bed       Freeboard
  IC_X_w           =  0.0             0.0
  IC_X_e           =  1.6             1.6
  IC_Y_s           =  0.0             5.0
  IC_Y_n           =  5.0            30.0
  IC_Z_b           =  0.0             0.0
  IC_Z_t           = @(2*Pi)         @(2*Pi)

  IC_EP_g          =  0.45            1.0

  IC_U_g           =  0.0             0.0
  IC_V_g           =@(45.8/0.45)     45.8
  IC_W_g           =  0.0             0.0

  IC_U_s(1,1)      =  0.0             0.0
  IC_V_s(1,1)      =  0.0             0.0
  IC_W_s(1,1)      =  0.0             0.0

  IC_P_star        =  0.0             0.0
  IC_T_g           = 300.0          300.0

#
#  Boundary Conditions Section
#
       !                 Grid     Exit
  BC_X_w           =     0.0      0.0
  BC_X_e           =     1.6      1.6
  BC_Y_s           =     0.0     30.0
  BC_Y_n           =     0.0     30.0
  BC_Z_b           =     0.0      0.0
  BC_Z_t           =    @(2*Pi) @(2*Pi)

  BC_TYPE          =    'MI'     'PO'

  BC_EP_g          =    1.0

  BC_U_g           =    0.0
  BC_V_g           =  200.0
  BC_W_g           =    0.0

  BC_P_g           = 1.013E6   1.013E6
  BC_T_g           = 300.0
```

```
#
#  Output Control
#
  RES_DT = 0.01
         !
         ! EP_g P_g       U_g  U_s  ROP_s     T_g  X_g
         !      P_star    V_g  V_s            T_s1 X_s    Theta  Scalar
         !                W_g  W_s            T_s2
  SPX_DT = 0.01 0.1       0.1  0.1  100.      100. 100.   100.0  100.0

  NLOG   = 100
  full_log = .true.
```

Vita

Mario Alberto Ruvalcaba was born on December 19th, 1984 in Juarez, MEXICO. The eldest son of Lilia Aurora Andrade Jimenez, he graduated from COBACH #6 High School in Juarez, MEXICO in 2002 and joined The University of Texas at El Paso (UTEP) in 2003 to pursue a Bachelor of Science in Mechanical Engineering. During this time he performed as a Science and Engineering Tutor for the Academic Center for Engineers and Scientists (ACES), in addition we worked as a Teaching Assistant for several engineering courses among them are Dynamics, Dynamic Response and Mechanical Design, he also taught one engineering course: Graphics and Engineering Design. After the completion of his Bachelor of Science in Mechanical Engineering he worked as a CFD engineer at Delphi Automotive Systems, at the same time he began attendance in the same university to pursue a Masters Degree in Mechanical Engineering. He started working at the Combustion and Propulsion Research Laboratory under the supervision of Dr. Ahsan Choudhuri where he currently performs.

Permanent address: 3211 Rancho Florido
Juarez, MEXICO, 32618

This thesis was typed by Mario A. Ruvalcaba